Photophysics of Clomeleon by FLIM: Discriminating Excited State Reactions along Neuronal Development

Mini Jose,* Deepak K. Nair,* Carsten Reissner,* Roland Hartig,[†] and Werner Zuschratter*
*Leibniz Institute for Neurobiology, Magdeburg, Germany; and [†]Medical Faculty, Otto-von-Guericke University, Magdeburg, Germany

ABSTRACT   In this work, fluorescence lifetime imaging microscopy in the time domain was used to study the fluorescence dynamics of ECFP and of the ratiometric chloride sensor Clomeleon along neuronal development. The multiexponential analysis of fluorophores combined with the study of the contributions of the individual lifetimes (decay-associated spectra) was used to discriminate the presence of energy transfer from other excited state reactions. A characteristic change of sign of the pre-exponential factors of lifetimes from positive to negative near the acceptor emission maxima was observed in presence of energy transfer. By fluorescence lifetime imaging microscopy, we could show that the individual conformations of CFP display differential quenching properties depending on their microenvironment. Suitability of Clomeleon as an optical indicator to obtain a direct readout of the intracellular chloride concentrations in living cells was verified by steady-state and time-resolved spectroscopy. The simultaneous study of the photophysical properties of Clomeleon, the calcium indicator Cameleon, and ECFP with neuronal development provided a kinetic model for the mechanism when competitive quenching effects as well as energy transfer occur in the same molecule. Simultaneous analysis of donor and acceptor kinetics was necessary to discriminate Försters resonance energy transfer along neuronal development due to the different cellular effects involved.

INTRODUCTION

A number of techniques have been developed so far to study the dynamic events taking place inside living cells. The complex organization of the cells makes it probable that the molecular behavior studied by artificial means and that in realistic conditions is not identical, and therefore is essential to study molecules in their natural environment (1). To study interactions in the nanometer scale with the light microscope, Försters resonance energy transfer (FRET) is utilized as a popular tool (2,3). The drastic fall in FRET efficiency with distance makes it an efficient tool for probing protein-protein interactions. When measuring in living cells, one of the major challenges is to overcome the concentration-dependence of measured parameters, whose determination is practically impossible in living cells. Fluorescence lifetime imaging microscopy (FLIM) monitors localized changes in the probe fluorescence lifetime that are independent of local fluorophore concentrations, but sensitive to environmental conditions such as pH and excited state reactions like FRET (4). Though FRET determination using lifetime imaging is currently utilized for studying interactions during different cellular signaling processes, the existence of the different molecular conformations of the fluorophores makes it difficult inside a living cell (5,6).

Monitoring the donor mean lifetimes alone does not give any information regarding the sources of individual lifetimes that could take part in energy transfer or in other excited state reactions. Time domain FLIM was used in this work to study FRET. Here, we have examined how the simultaneous detection and analysis of donor and acceptor molecules helped to overcome the foresaid problem to a great extent. The plots of pre-exponential factors or contributions of the different lifetimes of the donor and acceptor fluorophores as a function of wavelength (decay-associated spectra, i.e., DAS), were used to study the presence of FRET. This approach, which has been used successfully in solutions (7), was extended to biological samples where it allowed us to discriminate deviations in fluorescence properties of probes due to excited state reactions from other cellular effects.

Neuronal development is characterized by changes in intracellular ionic concentrations. In the immature brain, γ-aminobutyric acid (GABA) is excitatory. GABA becomes inhibitory by the delayed expression of a chloride exporter (KCC2), leading to a negative shift in the reversal potential for chloride ions (8). In the adult brain where Cl^- is the main mediator of synaptic inhibition, the shift in the nature of GABA is an essential feature to maintain equilibrium between excitation and inhibition to avoid pathological consequences. In this aspect, the studies in the changes of intracellular chloride concentrations during neuronal development play a major role. Making use of the high anionic sensitivity of YFP (9), a novel optical indicator called ''Clomeleon'' for studying the intracellular chloride concentrations was developed (10). In Clomeleon, a chloride-sensitive variant of YFP called Topaz (11) was linked with a relatively chloride-insensitive CFP using a 24 amino-acid linker to form a ratiometric chloride indicator. In this work, Clomeleon was used to study the changes in intracellular chloride concentrations during neuronal development.

The major challenges addressed in this work were:

1. Discrimination of FRET from other excited state reactions along neuronal development: It was essential to

understand the perturbation of donor lifetimes to the different photophysical processes to discriminate it from FRET. FRET-FLIM studies along neuronal development are challenging due to the different cellular effects involved, limiting the feasibility of this technique. To address this, DAS was used to characterize these changes with the help of simultaneous donor-acceptor detection and analysis. Here a multi-wavelength approach is presented, with which a discrimination of energy transfer from other excited state reactions was possible during development of living hippocampal neurons.

2. Investigation of the photophysics of Clomeleon at picosecond timescale: A detailed comparison of fluorescence emission dynamics of the donor alone (CFP) and of the FRET sample (Clomeleon) under different conditions was done, which included studies in purified solutions by varying chloride concentrations as well as pH levels. The effects observed were compared with an independent construct (namely Cameleon) containing a chloride-insensitive acceptor with a similar donor.

3. To ensure the suitability of Clomeleon as a ratiometric and lifetime indicator for chloride along development of living hippocampal neurons: Quantification of intracellular chloride concentrations at different stages of maturation of neurons using independent methods was adopted. This in turn allowed a direct correlation of the changes in the intracellular chloride concentrations to the maturation levels of individual neurons.

The simultaneous study of the photophysical properties of Clomeleon, the calcium indicator Cameleon, and ECFP with neuronal development were used to postulate a kinetic model for the mechanism when competitive quenching effects as well as energy transfer occur in the same molecule.

MATERIALS AND METHODS

Cell cultures, transfection, and immunocytochemistry

Primary hippocampal cultures were prepared according to the method of Goslin et al. (12) with some modifications. The hippocampal cells from E18 rat embryos were plated in Dulbecco's Modified Eagle's medium (Life Technologies, Karlsruhe, Germany) including 10% Fetal Calf Serum, antibiotics (100 U/ml penicillin, 100 μg/ml streptomycin), and 2 mM glutamine at a density of 80,000 cells per well (0.5 ml). Twenty-four hours after plating, the medium was exchanged for Neurobasal medium without phenol red (Life Technologies), containing 2% B27, 1% antibiotics, and 0.5 mM glutamine and incubated at 37°C, 5% CO_2 environment. COS-7 cells were grown in Dulbecco's Modified Eagle's medium including 10% Fetal Calf Serum, antibiotics (100 U/ml penicillin, 100 μg/ml streptomycin), and 2 mM glutamine at a density of 10^5 cells per well (0.5 ml) at 37°C, 5% CO_2 environment. Hippocampal neurons (days in vitro/DIV 7, 10, 14, 15) were transfected with ECFP, Cameleon, or Clomeleon (prk5 C24T) cDNAs using Lipofectamine 2000 (Life Technologies). COS-7 cells were transfected with ECFP or Clomeleon (prk5 C24T) cDNAs using PolyFect Transfection Reagent (Qiagen, Hilden, Germany). Neurons of DIV 7 and DIV 15 were fixed with 4% PFA in PBS and immunostained with anti-Bassoon mab7f (mouse, 1:1000, Stressgen, North Yorkshire, United Kingdom) and anti-

KCC2 (rabbit, 1:1000, Upstate, New York) as primary antibodies with Alexa 568 and Alexa 488 (anti-mouse/rabbit, 1:300, Molecular Probes, Eugene, OR) as secondary antibodies, respectively. Primary antibody incubation was done overnight at 4°C.

Purification of fluorescent proteins and digestion

The bacterial expression vectors, pQE30-Clomeleon (10) and pQE30-Cyan were expressed in *Escherichia coli* (XL1 blue) and their hexahistidine tags were used to purify the proteins via metal affinity chromatography (BD/ Clontech, Kelheim, Germany). FPLC (Superdex 200 column, GE Healthcare Life Sciences, Freiburg, Germany) was done to select the fraction containing the best ratio of Clomeleon to the cleaved single CFP and Topaz molecules. A buffer containing 147 mM Na^+ gluconate, 10 mM HEPES, 0.1% TWEEN 20, 0.025% Na Azide pH 7.4 with osmolarity adjusted to 305 mOsm/l with K^+ gluconate was used for the purpose. Micro Amido Black protein assays showed the protein concentrations to be 20 ng/μl for the fractions selected for the optical measurements. Purified Clomeleon was digested with rTEV protease (Life Technologies) in the recommended conditions to yield >90% of cleaved protein, as shown by Western blots.

Three-dimensional modeling of Clomeleon

The structure of Clomeleon and of its fluorescent N- and C-terminal domains is not known. Therefore, the structure of Clomeleon was built by homology modeling. Each domain and linker sequence was analyzed by a NCBI BLASTp search against structures from the protein data bank PDB (http://www.rcsb.org, (13)). The resulting aligned sequence fragments were modeled by blast2model (14). Finally, the structure of Clomeleon was constructed using PDB entries 1QA, 1PGY, and 1GFP as templates for CFP, the rTEV site, and YFP, respectively. The two fluorescent domains of Clomeleon are likely to build a close heterodimeric arrangement. Currently, 12 dimeric structures of fluorescent proteins are listed in the PDB. To increase the number, a library of template dimer structures was built by selecting potential dimer pairs from a data set of crystal-symmetry-related molecules calculated for 50 different crystal structures of fluorescent proteins, all members of the GFP β-barrel folding class. For each template, the premodeled domains were arranged accordingly and the glycine-serine linker was fit using a PDB loop database (13). The interface was positionally refined (15,16) and validated by programs WHAT IF (17) and PROCHECK (18). The aim of the modeling was to restrain the coordinates of the fluorescent domains, but build the most compact structural complex. Experimental dimers of fluorescent proteins are in antiparallel or crosslike orientation. For comparison, a parallel oriented heterodimer was arranged manually and the interface refined.

Steady-state imaging

The neurons were imaged in an extracellular buffer 1×KD (pH 7.4, 129 mM NaCl, 5 mM KCl, 2 mM CaCl₂ 2H₂O, 1 mM MgCl₂ 6H₂O, 20 mM HEPES, 30 mM Glucose). The microscope was equipped with a charge-coupled device (CCD) camera (F View, SIS Imaging Systems, Duesseldorf, Germany) connected to the top port of the microscope (Fig. 1). Mirror M3 was used to alternate between mercury lamp excitation coupled by an optical fiber and the laser illumination. The CFP and Topaz signals were collected by filter settings (all from AHF Analysentechnik, Tübingen, Germany), D436/20 excitation filter, 455 DCLP dichroic beam splitter, and D480/40 emission filter for CFP and HQ 500/20 excitation filter, Q515 LP dichroic beam splitter, and HQ 535/30 emission filter for Topaz. Only the cells showing moderate expression levels of the transfected constructs were used for imaging. The captured images gave an account of the morphology of the cells that were measured. To regulate the intracellular chloride concentrations, COS-7 cells were incubated in gluconate buffers containing varying amounts of chloride (0, 30, and 50 mM) along with 100 μM Nigericin
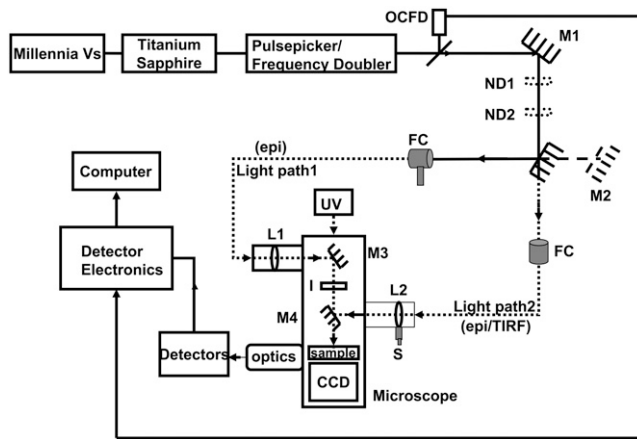
FIGURE 1 Experimental setup to study picosecond FLIM and FRET using point and imaging detectors in the epifluorescence and TIRF modes. *OCFD*, optical constant fraction discriminator triggered by laser pulse; *M*, mirrors; *ND*, neutral density filters; *UV*, mercury lamp for steady-state imaging; *FC*, optic fiber coupler; *epi*, epifluorescence mode; *TIRF*, total internal reflection fluorescence mode; *L*, planar convex lens; *I*, iris to control the area of excitation of the sample; *S*, micrometer screw, and *CCD*, charge-coupled device for steady-state imaging.

(Sigma Aldrich, Seelze, Germany) and 50 μM Tributyltin chloride (TBTC) (Sigma Aldrich) for 13–17 min. The buffers were changed in between to ensure stabilization of intracellular ionic concentrations. The purified proteins were mixed with varying concentrations of KCl to yield 0–50, 100, 250, and 500 mM Cl$^-$. Equal amounts of proteins were used in all cases to avoid differences in excitation conditions. pH studies of purified proteins were done using suitable buffering conditions from pH 6.0–8.0 at 0 mM Cl$^-$. Confocal images of neurons (DIV 7 and DIV 15) immunostained with antibodies against KCC2 and Bassoon were captured using Leica-TCS-SP2-AOBS (Leica Microsystems, Bensheim, Germany).

FLIM system

The experimental setup to study picosecond FLIM and FRET using ultrasensitive detectors in the epifluorescence and TIRF modes is depicted in Fig. 1. A femtosecond mode-locked Titanium sapphire laser (Tsunami Model 3955, 690–1080 nm; 80 MHz, Spectra Physics, Mountain View, CA) pumped by a continuous diode laser (Millennia Vs, 5W, TEM$_{00}$ 532 nm, Spectra Physics), was tuned and frequency-doubled using a frequency doubler/pulse picker (Model 3986, Spectra Physics) to a desired wavelength of 420 nm with a pulse repetition rate of 8 MHz. The excitation probability at this wavelength was >80% for the donor CFP whereas, for the acceptor Topaz, it was <5% (19). Approximately 10% of the laser output from the frequency doubler/pulse picker was used to trigger an Optical Constant Fraction Discriminator (OCFD 401, Becker and Hickl, Berlin, Germany) to provide the stop pulse to the electronics of the detectors. The laser beam was guided by mirror M1 to two circular variable neutral density filters ND1 and ND2 (Thorlabs, Karlsfeld, Germany), arranged in series to control the power of the laser beam. The laser beam was coupled alternatively via two optical fibers with the fiber couplers (*FC*) mounted on three-dimensional micrometer stages (Thorlabs) to different ports of an inverted microscope (IX81, Olympus, Hamburg, Germany). This allowed illumination of the sample for the two types of detectors used, either via light path 1 or 2. Manually switchable mirrors M2 and M4 were used to alternate between the illumination paths.

The Delay line and Quadrant anode (QA) detectors (20) (Europhoton, Berlin, Germany), based on time- and space-correlated single photon counting were used to study the interaction between tagged fluorophores by simultaneous acquisition of time and space information at picosecond scale. Here statistical averaging of the acquired single photons in time was done.

The Delay line (point) detector was used to analyze statistically a very small area of the sample (5–10 μm) and to resolve spectrally the corresponding fluorescence decays using a polychromator placed in front of the detector. Time correlation was done by measuring the delay between the current pulse generated from the second multichannel plate of the detector and the signal from the OCFD triggered by the excitation beam. Thus, the multiparameter data acquisition translated time and space coordinates into an intensity-dependent color contour with 256 space channels and 1024 time channels.

To illuminate the sample for the point detector via light path 1, the collimated laser beam from the fiber output was focused by a convex lens L1 ($f = +150$ mm, Edmund Optics, Karlsruhe, Germany), decreasing the area of illumination for the excitation beam. The region of interest was selected by closing an iris (I) within the excitation path around the beam to limit the area of excitation. The laser beam was finally focused onto the sample using an oil immersion 100× objective (Plan Apo 100×/1.45 oil, TIRFM, Olympus) after passing a beam splitter 450 DCLP. The fluorescence from the tiny selected area passed the emission filter HQ 460 ALP and the slit (11 mm × 0.10 mm) of the polychromator fixed in front of the sensitive area of the point detector to translate the spectrally resolved intensity decays on the detector.

In light path 2, the collimated beam from the optical fiber was used to provide whole-field illumination for the QA (imaging) detector. The fluorescence decays within the whole-field illuminated region were imaged simultaneously in this case. Time correlation was done similar to the point detector. Time- and space-correlated data were recorded as a three-dimensional matrix of 512 × 512 space channels and 4096 time channels.

The collimated beam in light path 2 passed the beamsplitter 450 DCLP and illuminated the back focal plane of the 100× objective. The fluorescence was collected via the objective and was reflected to the side port of the microscope after passing an emission filter HQ 460 LP. In front of the imaging detector, a Dual Image (Europhoton) was mounted to split the fluorescence into two specific wavelength bands via a beamsplitter (dichroic 505 DCXR). Two bandpass filters defined the width of the donor (CFP: D 480/40 M) and the acceptor (YFP: 540/40 ALP) channels. These fluorescence bands illuminated corresponding areas on the imaging detector, thereby collecting the dynamics of the donor and acceptor fluorophores simultaneously.

A possibility to alternate between epifluorescence and TIRF illuminations was also feasible in light path 2. This was provided by a micrometer screw *S* attached to a collimating lens (*L2*), which allowed to change the angle of incidence of the excitation beam from epifluorescence mode to TIRF mode, where the beam undergoes total internal reflection at the glass-buffer interface.

The QA capture software was used to control the data acquisition of the imaging detector. Measurements were performed by continuously acquiring the photons for a certain time (15–25 min) to achieve a good signal/noise ratio. The imaging detector was cooled throughout the measurements between 14 and 16°C to avoid overheating.

Calibration of the setup

The pulse-width of the instrument response function in the point detector was reduced to a minimum of 150 ± 25 ps measured at full width half-maximum by adjusting the threshold and zero control of the OCFD. Optimum excitation intensities at the sample <100 μW/cm^2 (measured by a laser power meter, PD-300-3W, Ophir Optronics, Rohrsen, Germany) was chosen to minimize phototoxicity of cells during measurement.

Wavelength calibration of the point detector was performed using a Xenon lamp (6035 Hg (Ar), Oriel Instruments, Stratford, CT). The wavelength sensitivity of the system was characterized to be 1.02 nm/channel. The time calibration of the point detector was performed by measuring the

instrument response function at different known delays. The time-channel resolution of the point detector was calculated to be 24.81 ps/channel.

The pulse width of the instrument response function in the imaging detector was reduced to a minimum of 200 ± 20 ps at full width half-maximum. The space calibration of the imaging detector was performed using fluorescent beads of 1 μm and 0.17 μm diameters (Ps-Speck, Molecular Probes). Time calibration of the imaging detector was performed similar to the point detector and the time-channel resolution was calculated to be 9.72 ps/channel.

Independent control measurements of the monoexponential dye coumarin6 in ethylene glycol at magic angle, excited at 420 nm and observed in a band of 515 ± 15 nm (HQ 515/30), was performed with both point and imaging detectors.

Data analysis

The fluorescence emission spectra obtained from the point detector were normalized to the emission peak of CFP and the R-values were calculated as the ratio of intensities at the emission maxima of Topaz to CFP.

The fluorescence decays were analyzed by Levenberg-Marquardt nonlinear least-squares algorithm using the Globals Unlimited software package (Ver. 1.20 (21)). The decays were modeled by the convolution product of a multiexponential theoretical model with the instrument response function (IRF): $i(t) = IRF(t) \otimes \Sigma \alpha_i e^{-t/\tau_i}$, where α_i is the relative contribution of fluorescent species characterized by the fluorescence lifetime τ_i and IRF is the pulsed excitation obtained by acquiring the reflection of the laser beam to the detector. The quality criterion for global fit was defined as $\chi^2 < 1.3$ for all analyzed decays. The criterion for improvement of χ^2 on addition of multiexponential components were set to a value of $\Delta \chi^2$, the ratio between the χ^2 values of the previous model and the current model on addition of a single lifetime component, where $\Delta \chi^2 > 1.05$. χ^2 was checked using the linked multiexponential model and the unlinked model, and the data set was discarded if the ratio of χ^2 values was > 1.05, indicating a random error originating from the data acquisition.

Data obtained from the point detector were fit with linked lifetimes along different decays corresponding to different emission wavelengths. The individual decays were obtained by binning data over a fixed number of continuous wavelength channels, resulting in a net resolution of 6.12 nm per decay. The contributions of the multiple lifetimes in the intensity decays were obtained as pre-exponential factors α_i. The pre-exponential factors of lifetimes were positive except in the case of excited state reactions, where they change to negative (22). The α_i-values obtained from the individual decays were plotted as a function of wavelength to obtain the decay-associated spectra (DAS). The comparison of DAS of different multiexponential components allowed us to discriminate fluorescent species involved in different excited state processes. DAS was also used to deduce the fractional contributions of the different lifetimes along the wavelength, from the pre-exponential factors as $|\alpha_i|/\Sigma|\alpha_i|$. The mean lifetime of a multiexponential fluorophore was calculated as $\tau_{mean} = \Sigma|\alpha_i \tau_i|/\Sigma|\alpha_i|$, where τ_i is the lifetime and α_i is the corresponding pre-exponential factor. The individual counts at the peak for each analysis was maintained between 6000 and 7000.

The FRET efficiency was calculated using $E_i = 1 - \tau_{DA}/\tau_D$ where τ_D is the unperturbed lifetime of the donor and τ_{DA} is the lifetime of the donor in the presence of an acceptor, which in turn allowed the determination of the distance between the fluorophores from $d = d_0(1/E-1)^{1/6}$, where d_0 is 49.2 Å for CFP-YFP pairs (23). The distance calculations were done assuming a random orientation for the dipole moments, with $\kappa^2 = 2/3$.

Data obtained from the imaging detector were analyzed by selecting corresponding regions of interest (ROIs) for the CFP and Topaz channels. The data sets of individual channels were exported to the Globals Unlimited software format. The donor and acceptor decays were analyzed with linked lifetimes. For comparing the decay differences at different intracellular compartments of cells, the peak counts were always ensured to be $> 10^4$.

The intensity decays of coumarin6 at magic angle were observed to be monoexponential with lifetimes of 2.30 ns for the point detector and 2.29 ns

for the imaging detector, comparable to the published value of 2.30 ns (24). This was done to ensure that the effects observed were purely cellular.

RESULTS

1. One of the major challenges addressed in this work was to discriminate FRET from other excited state reactions along neuronal development. To do so, it was important to understand the deviations in the properties of the donor under varying microenvironments. Therefore, the fluorescence dynamics of purified CFP was studied under different pH and chloride conditions. The effects were compared with ECFP expressed at different stages of neuronal maturation.

Fluorescence dynamics of CFP in solution

The fluorescence emission maximum of purified CFP was observed at 486 nm, which was stable under varying pH and chloride conditions (Fig. 2 *a*). With lowering of pH levels, the contribution of the red-shifted shoulder of CFP at 505 nm was found to increase. The fluorescence decay of CFP was biexponential at pH levels >7.0, with lifetimes of 3.26 ± 0.10 ns (τ_1) and 1.12 ± 0.03 ns (τ_2). The presence of a third short lifetime component of 0.28 ± 0.06 ns (τ_3) was observed at acidic pH levels with τ_1 and τ_2 changed to 3.09 ± 0.09 ns and 1.38 ± 0.08 ns, respectively, which significantly affected the overall fluorescence decay of CFP (Fig. 2 *b*). The lifetimes τ_1 and τ_3 showed clear deviations in their individual contributions at varying pH levels, whereas τ_2 remained unaffected (Fig. 2 *c*). This resulted in an overall increase in the mean lifetime of CFP with increasing pH (Fig. 2 *d*). The effects of chloride on the fluorescence dynamics of CFP were minimal and are therefore not presented. A small increase in the donor mean lifetime from 2.36 ns to 2.49 ns was observed on increasing the chloride levels from 0 mM to 500 mM.

The fluorescence dynamics of CFP was significantly affected by pH in contrast to chloride.

Fluorescence dynamics of ECFP in hippocampal neurons

To determine the suitability of the donor at different maturational stages, living hippocampal neurons expressing ECFP were measured at three different stages namely DIV 7, 10, and 15. ECFP showed the emission maximum at 486 nm (Fig. 3 *a*) irrespective of the developmental stage of cells, though a difference in the contribution of its second peak at 505 nm was observed with development.

The fluorescence decay of ECFP measured at DIV 7 was fit with three lifetime components of 3.39 ± 0.04 ns (τ_1), 1.4 ± 0.13 ns (τ_2), and 0.29 ± 0.04 ns (τ_3), showing comparable contributions ($N = 3$, Table 1, Fig. 3 *b*). The DAS revealed a
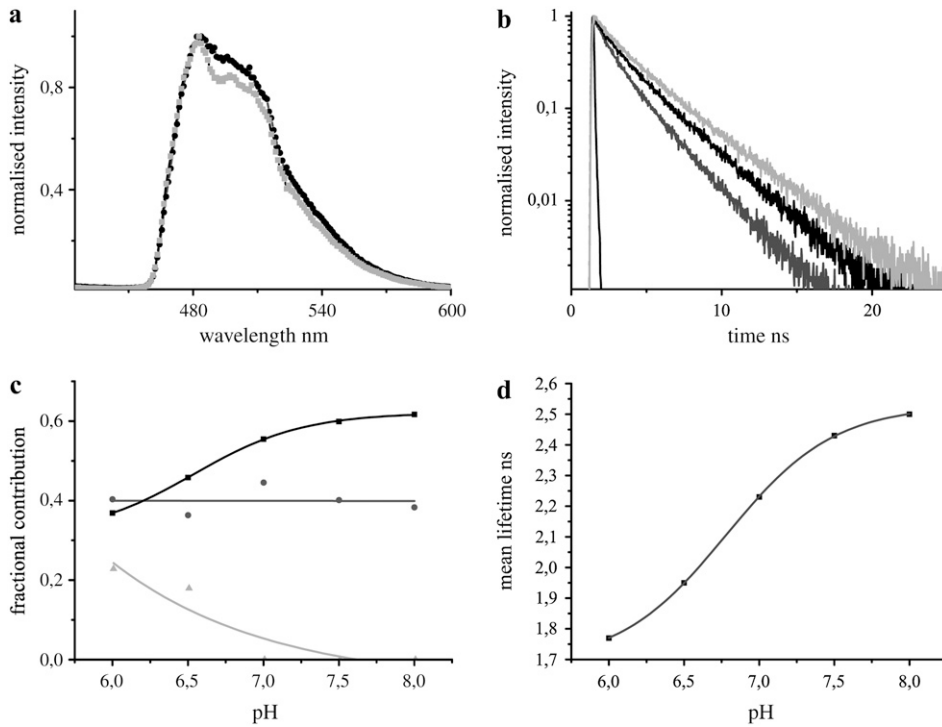
FIGURE 2 The fluorescence characteristics of purified CFP in solution at 420 nm excitation under varying pH conditions. (*a*) Comparison of fluorescence emission spectra of CFP at pH 6.5 (*dark shading*) and at pH 7.5 (*light shading*). The fluorescence maxima were observed at 486 nm irrespective of the pH levels, though a difference in the contribution of the second peak at 505 nm was observed. (*b*) The fluorescence decays of CFP at pH 6.0 (*shading*), 6.5 (*dark shading*), and 8.0 (*light shading*). (*c*) The contributions of the lifetimes τ_1 (*solid*), τ_2 (*shading*), and τ_3 (*light shading*) at the donor emission maximum were calculated from the pre-exponential factors and plotted as normalized fractional contributions as a function of pH. (*d*) Mean lifetimes at the donor emission maximum were plotted as a function of pH.

similar spectral spread for all the three lifetimes (Fig. 3 *c*). The mean lifetime of ECFP at its emission maximum was 1.76 ± 0.13 ns, which remained constant along the spectra.

At DIV 10, ECFP was still observed to be three-exponential, though with a slight difference in the individual lifetimes as well as their contributions ($N = 5$, Table 1). The contribution of τ_1 was increased with a simultaneous

reduction for τ_3, compared to DIV 7. The contribution of τ_2 remained unchanged. DAS was also similar for the two stages. The mean lifetime of ECFP at DIV 10 was increased to 1.97 ± 0.10 ns (Table 1), though its spectral spread was similar to that observed at DIV 7.

At DIV 15, the total cell population was split up into two categories based on their intensity decays, 60% showing a
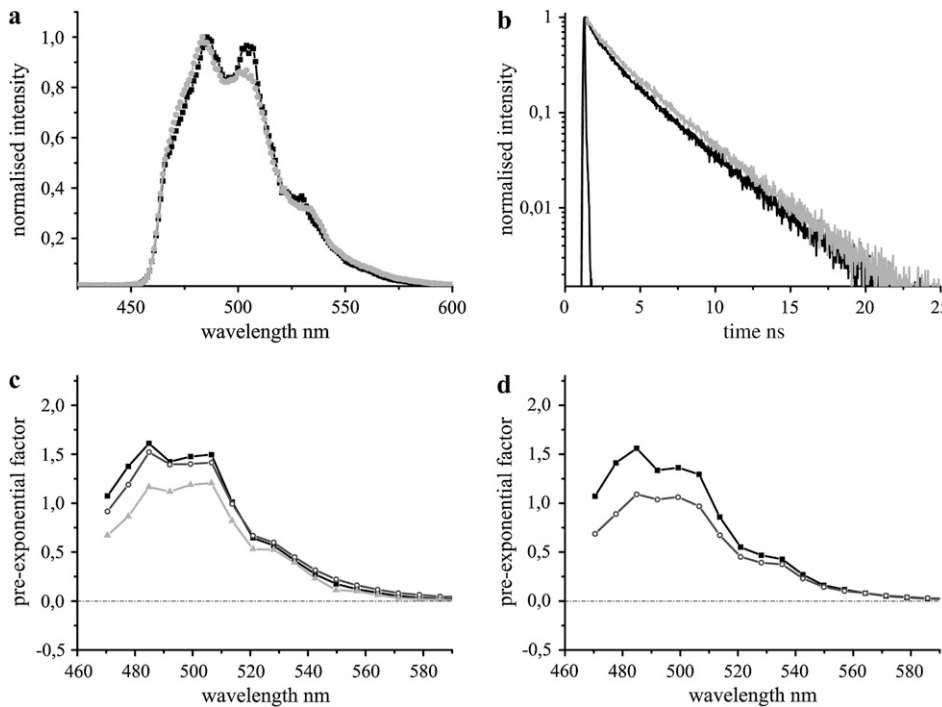

FIGURE 3 The fluorescence emission dynamics of ECFP at 420 nm excitation in hippocampal neurons. (*a*) Comparison of fluorescence emission spectra of ECFP at DIV 7 (*dark shading*) with DIV 15 (*light shading*). The fluorescence maxima were observed at 486 nm, though a difference in the contribution of the second peak at 505 nm was observed. (*b*) Comparison of fluorescence decays of ECFP at DIV 7 (*dark shading*) with DIV 15 (*light shading*). IRF is shown in solid representation. The former was fit by a three-exponential model, whereas the majority of cells at DIV 15 displayed only two lifetimes (Table 1). (*c*) DAS of ECFP at DIV 7. Intensity decays were analyzed in 20 emission bands from 470 nm to 590 nm and the pre-exponential factors of lifetimes τ_1 (*solid*), τ_2 (*shading*), and τ_3 (*light shading*) were plotted along the wavelength. (*d*) DAS of biexponential ECFP at DIV 15. The pre-exponential factors of lifetimes, τ_1 (*solid*) and τ_2 (*shading*), were plotted along the wavelength.

TABLE 1 Fluorescence emission dynamics of ECFP at different maturational stages of hippocampal neurons

Cell	DIV	τ_1 (ns)	τ_1 (%)	τ_2 (ns)	τ_2 (%)	τ_3 (ns)	τ_3 (%)	τ_{mean} (ns)
Neurons	7	3.39 ± 0.04	35 ± 3	1.4 ± 0.13	35 ± 1	0.29 ± 0.04	30 ± 4	1.76 ± 0.13
	10	3.36 ± 0.05	44 ± 3	1.36 ± 0.07	33 ± 1	0.19 ± 0.03	23 ± 3	1.97 ± 0.10
	15	3.45 ± 0.14	37 ± 2	1.50 ± 0.26	34 ± 5	0.23 ± 0.14	28 ± 3	1.96 ± 0.15
	15	3.30 ± 0.02	59 ± 1	1.08 ± 0.04	41 ± 1			2.38 ± 0.03
COS-7		3.26 ± 0.05	57 ± 1	1.06 ± 0.03	43 ± 1			2.31 ± 0.05

The multiple lifetimes and individual contributions of ECFP are shown at different stages of neuronal development. The percentage of contributions of τ_1, τ_2, and τ_3 are denoted as τ_1%, τ_2%, and τ_3%, respectively. The major fraction of cells at DIV 15 (60%) displayed biexponential decay for ECFP in contrast to young stages. COS-7 cells showed lifetimes and contributions similar to the majority of mature neurons.

typical biexponential fit of ECFP (Fig. 3 *b*) with lifetime components of 3.30 ± 0.02 ns (τ_1) and 1.08 ± 0.04 ns (τ_2), whereas the rest showed a three lifetime fit similar to DIV 7 and DIV 10 (*N* = 10, Table 1). DAS was also similar for both the categories compared to the previous stages, with the exception of the absence of τ_3 for the majority of neurons at DIV 15 (Fig. 3 *d*). The mean lifetimes of ECFP at the emission maximum were 2.38 ± 0.03 ns and 1.96 ± 0.15 ns for the first and second categories, respectively, with their spectral spread similar to those at younger stages (Table 1). DAS of ECFP at all stages of neuronal development showed only positive values for the pre-exponential factors of the multiple lifetimes (Fig. 3, *c* and *d*).

The decay kinetics of ECFP was measured in COS-7 cells to check for cell-to-cell variability of lifetimes. In this case, the decays were fit using a two-exponential model of 3.26 ± 0.05 ns and 1.06 ± 0.03 ns, yielding a mean lifetime of 2.31 ± 0.05 ns at its emission peak (*N* = 5, Table 1).

The fluorescence dynamics of the popular donor probe ECFP, previously assumed to be insensitive to developmental changes, was altered with maturation of hippocampal neurons.

2. Clomeleon is a ratiometric indicator for chloride with CFP and Topaz separated by 24 amino acids. Since the donor CFP was observed to be significantly affected by pH, it was essential to study the fluorescence properties of Clomeleon individually under varying chloride and pH conditions for a detailed understanding of its photophysics. Clomeleon was digested with a protease capable of efficiently cleaving it into individual CFP and Topaz molecules. The study of the digested sample under the varying foresaid conditions allowed a better understanding of the effects on single CFP and Topaz fluorophores making the construct. The reliability of the measurements was verified by molecular modeling. The observations were compared with Clomeleon and Cameleon at different stages of maturation of hippocampal neurons.

Fluorescence characteristics of Clomeleon in solution

Varying chloride levels

Purified Clomeleon was measured by varying the chloride concentrations from 0 to 50, 100, 250, and 500 mM at pH

7.4. The intensity ratios of Topaz to CFP at their emission peaks, measured as *R*, were plotted for the corresponding chloride concentrations (Fig. 4 *a*), with values ranging from 1.7 for 0 mM down to 0.8 and 0.5 for 50 mM and 500 mM Cl⁻, respectively. *R*-values reduced exponentially with increasing chloride concentrations, which saturated above 100 mM (Fig. 4 *a*). The fluorescence decay of Clomeleon in solution was fit by a three-exponential model with lifetimes of 3.37 ± 0.02 ns (τ_1), 1.33 ± 0.03 ns (τ_2), and 0.21 ± 0.02 ns (τ_3), except for 0 mM Cl⁻, which showed 2.82 ns (τ_1), 0.97 ns (τ_2), and 0.21 ns (τ_3). Though the lifetimes of Clomeleon were not changed on varying the chloride concentrations (>0 mM), differences in the fractional contributions of the individual lifetimes were observed. The contribution of τ_1 increased with increasing chloride concentrations from 18% to 41% at the donor emission maximum, whereas that of τ_3 decreased from 43% to 25% at the same. τ_2 showed only a slight change in its contribution from 39% to 34%. The plots of all the three lifetime contributions on varying the chloride concentrations were fit with single-exponential functions ($y_0 + A_1 e^{(x/t_1)}$) (Fig. 4 *b*). Consequently, the Stern-Volmer plot displayed a drastic increase in the donor mean lifetimes on increasing the chloride levels (Fig. 4 *c*). At the acceptor emission maximum a reverse effect was seen, where the contribution of τ_1 decreased from 89% to 66% with a simultaneous increase in contributions of τ_2 and τ_3 from 9% and 2% to 22% and 12%, respectively. This resulted in an exponential decrease in the acceptor mean lifetime of Clomeleon from 3.15 ns to 2.54 ns on increasing the chloride concentrations.

Varying pH levels

Purified Clomeleon was measured at different pH levels in the physiological range from 6.0 to 8.0. At 0 mM Cl⁻, *R*-values drastically decreased from 1.64 ± 0.08 to 0.76 ± 0.01 on lowering the pH levels (Fig. 4 *d*). The fluorescence decay of Clomeleon was fit with three lifetimes at all pH conditions. Lifetimes of 3.09 ± 0.07 ns (τ_1), 1.20 ± 0.08 ns (τ_2), and 0.19 ± 0.06 ns (τ_3) were observed at pH < 7.0, which changed to 2.84 ± 0.03 ns (τ_1), 0.93 ± 0.06 ns (τ_2), and 0.17 ± 0.06 ns (τ_3) at higher pH levels. The contributions of the individual lifetimes were affected on varying the pH, with τ_1 and τ_3 showing significant changes,
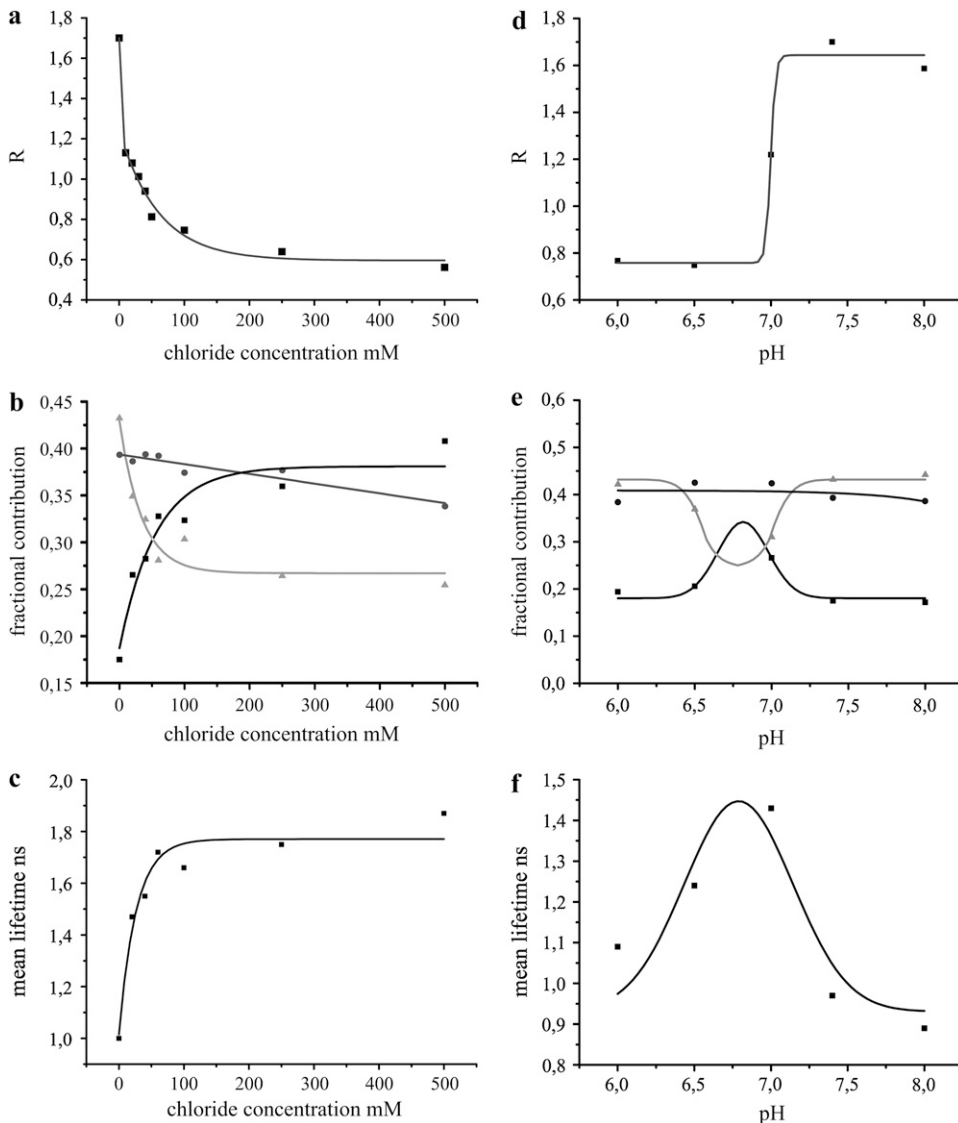
FIGURE 4 Fluorescence properties of purified Clomeleon in solution under varying chloride and pH conditions. (*a*) *R*-values of purified Clomeleon at different chloride concentrations. *R*-values reduced exponentially on increasing the chloride concentrations. (*b*) The contributions of lifetimes τ_1 (*solid*), τ_2 (*shading*), and τ_3 (*light shading*) at the donor emission maximum were calculated from the pre-exponential factors and plotted as normalized fractional contributions with increasing chloride concentrations. The contributions of τ_1 and τ_3 were most affected in contrast to τ_2. (*c*) The mean lifetimes of Clomeleon at the donor emission maximum increased exponentially with increasing chloride concentrations, yielding the Stern-Volmer plot. (*d*) *R*-values of purified Clomeleon at different pH levels. *R*-values reduced drastically at acidic pH levels. (*e*) The fractional contributions of the lifetimes τ_1 (*solid*), τ_2 (*shading*), and τ_3 (*light shading*) at the donor emission maxima were plotted as a function of pH. The contributions of τ_1 and τ_3 were most affected in contrast to τ_2. (*f*) The donor mean lifetimes of Clomeleon showed a Gaussian fit with high quenching effects at acidic pH levels and high FRET at pH >7.3.

whereas minor deviations were observed for τ_2 (Fig. 4 *e*). Consequently, the donor mean lifetimes showed a Gaussian distribution on varying the pH conditions (Fig. 4 *f*). A reverse effect for the fractional contributions of the acceptor lifetimes was observed on varying the pH levels. The contributions of τ_1 increased at approximately pH 6.9 with a simultaneous decrease for τ_2 and τ_3 at the same, resulting in an increase in the acceptor mean lifetime from 1.80 ns to 2.94 ns.

The fluorescence dynamics of Clomeleon was drastically affected by pH and chloride, with FRET decreasing both at high chloride concentrations and low pH levels.

Clomeleon in presence and absence of rTEV protease

Purified Clomeleon was digested with rTEV protease, which recognized the ENLYFQG sequence at the center of the linker connecting the CFP and Topaz fluorophores. This yielded the 28 kDa band instead of the 57 kDa band of undigested Clomeleon in the Western blot (Fig. 5 *c*). Greater than 90% cleavage of Clomeleon was observed after digestion. The fluorescence spectra as well as decay of Clomeleon were altered on protease digestion (Fig. 5, *a* and *b*). The *R*-value of purified Clomeleon at 0 mM Cl$^-$ (pH 7.4) was measured to be 1.7, which reduced to 0.42 in presence of the protease.

The fluorescence decay of Clomeleon after protease digestion was fit by a two-exponential model with lifetime components of 3.43 ± 0.02 ns (τ_1) and 1.02 ± 0.02 ns (τ_2), irrespective of the chloride concentration used. Compared to the undigested Clomeleon at 0 mM Cl$^-$ and pH 7.4, at the donor emission maxima, the contribution of τ_1 was increased to 64% from 18% whereas that of τ_2 slightly reduced to 36% from 39% on digestion. Consequently, the overall donor fluorescence decay of the digested sample was longer compared
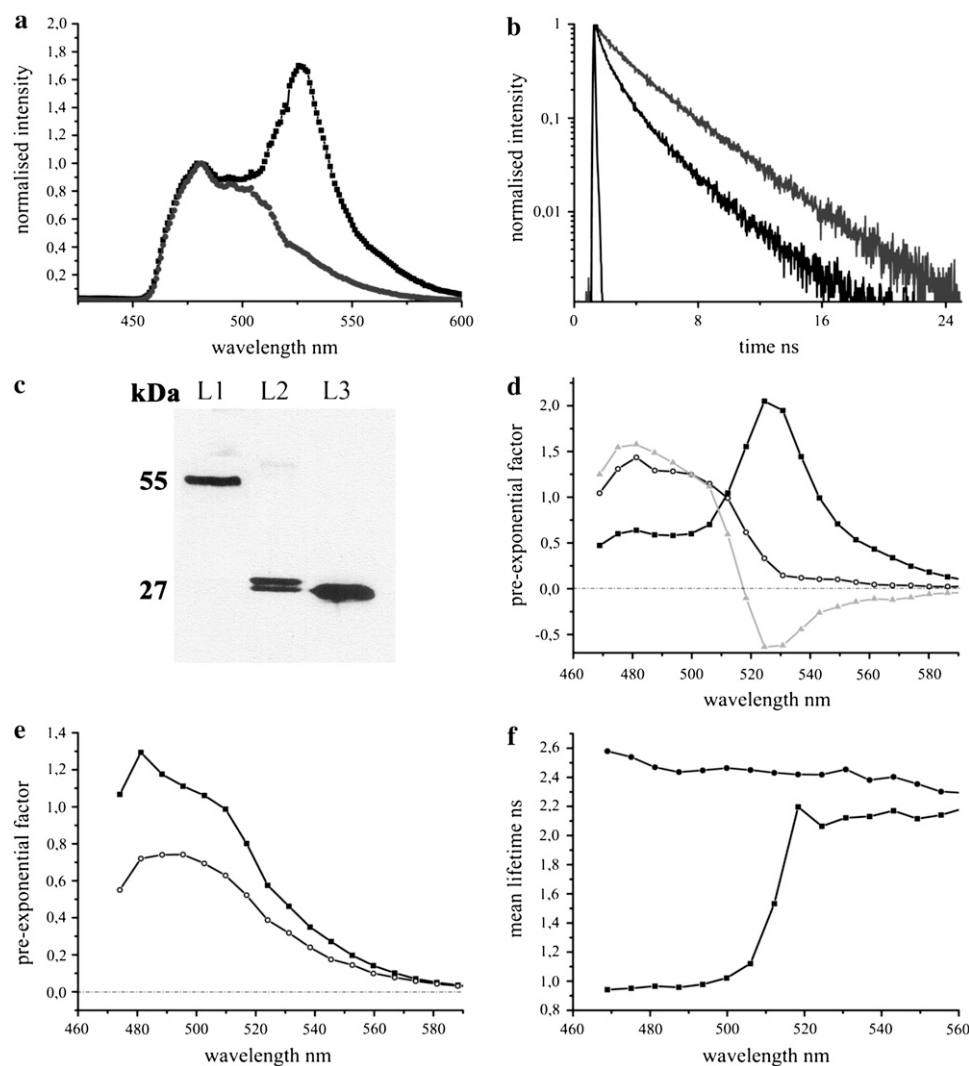
FIGURE 5 The fluorescence emission dynamics of purified Clomeleon before and after protease digestion. (a) Comparison of fluorescence emission spectra of Clomeleon before (dark shading) and after (shading) protease digestion. The R-value of Clomeleon at 0 mM Cl⁻ and pH 7.4 was reduced from 1.7 to 0.42 on digestion. (b) Comparison of fluorescence decay of digested Clomeleon (shading) with the undigested (dark shading). Decay of the former was observed to be longer compared to the latter. (c) Western blot showing the digested protein band of 28 kDa (L2) compared to the undigested Clomeleon of 57 kDa (L1). Control GFP protein is shown in L3. (d) DAS of undigested Clomeleon. The pre-exponential factors of τ_3 (light shading) displayed negative values at the acceptor emission maximum. (e) DAS of Clomeleon after protease digestion. The pre-exponential factors of τ_1 (solid), and τ_2 (shading) were positive similar to CFP. (f) Mean lifetimes of undigested (solid square) and digested Clomeleon (shaded circle).

to the undigested control (Fig. 5 b). At 0 mM Cl⁻, DAS of undigested Clomeleon displayed negative pre-exponential factors of τ_3, whereas only positive amplitudes were observed for all the lifetimes similar to CFP after digestion, indicating the absence of energy transfer even in presence of single CFP and Topaz molecules in the same stoichiometry (Fig. 5, d and e). The contributions of the individual lifetimes also exhibited differences in their spectral spread. For the undigested FRET sample, τ_1 showed a drastic increase in its contribution along the spectra with a simultaneous decrease for τ_2 and τ_3. This was in contrast to the digested Clomeleon, which revealed no changes along the spectra. Consequently, after protease digestion the mean lifetime at the donor emission maximum increased from 0.97 ns to 2.54 ns similar to CFP (Fig. 5 f). Only a minor increase in the donor mean lifetime from 2.54 ns to 2.63 ns was observed on increasing the chloride concentrations from 0 mM to 500 mM for the digested sample. On varying the pH levels for the digested sample, similar changes to that observed for CFP alone was

observed with no additional contributions in the acceptor channels.

FRET was completely absent for the protease-digested Clomeleon, with its fluorescence dynamics similar to CFP on varying the chloride and pH levels.

Modeling of Clomeleon

Using τ_1 of purified CFP (0 mM Cl⁻, pH 7.4) of 3.21 ns, which is most affected by quenching, as the unperturbed donor lifetime in the absence of acceptor and τ_3 of purified Clomeleon of 0.21 ns as the perturbed lifetime of donor in presence of the acceptor or the FRET lifetime (0 mM Cl⁻, pH 7.4), the intramolecular distance between the CFP/Topaz chromophores in Clomeleon was calculated. The value d_0 was fixed to be 49.2 Å for CFP-YFP pairs (23) and a random orientation of dipole moments with $\kappa^2 = 2/3$ was assumed. This yielded a FRET efficiency of 94%, which resulted in the interchromophore distance d to be 32 Å. Since there was

equal probability for the FRET lifetime of 0.21 ns to be arising from the quenching of τ_2 of CFP (1.1 ns), such a calculation yielded the efficiency to be 80% and consequently the distance d to be 39 Å. Both the calculated distances were in agreement with the theoretically calculated values from molecular modeling of 33 Å (Fig. 6).

Energy transfer dynamics of Clomeleon at different developmental stages of hippocampal neurons

To get an overall understanding of the changes in the intracellular chloride concentrations of neurons during maturation, the biophysical properties of the ratiometric indicator Clomeleon were studied at four different developmental stages of neurons—namely DIV 7, 10, 14, and 15. The fluorescence emission spectra of Clomeleon at all stages showed the CFP emission maximum at 486 nm and the corresponding Topaz emission at 527 nm (Figs. 7 a and 8 a). Neurons were classified based on individual Topaz/CFP intensity ratios at their emission peaks (R) into class I, class II, and class III with R-values of 0.4–0.8, 0.8–1.2, and 1.2–1.6, respectively.

The fluorescence spectra of Clomeleon at DIV 7 revealed a quenched Topaz emission relative to CFP (Fig. 7 a), with cells falling into class I of R-values in the range of 0.42 ± 0.04 ($N = 10$). A representative cell is shown in Fig. 7 c. The fluorescence decay of Clomeleon at this stage was fit by a three-exponential model with lifetimes of 3.39 ± 0.05 ns (τ_1), 1.35 ± 0.06 ns (τ_2), and 0.26 ± 0.03 ns (τ_3), with the maximum contribution observed for τ_1 at the donor emission peak ($N = 5$, Table 2). The overall donor fluorescence decay
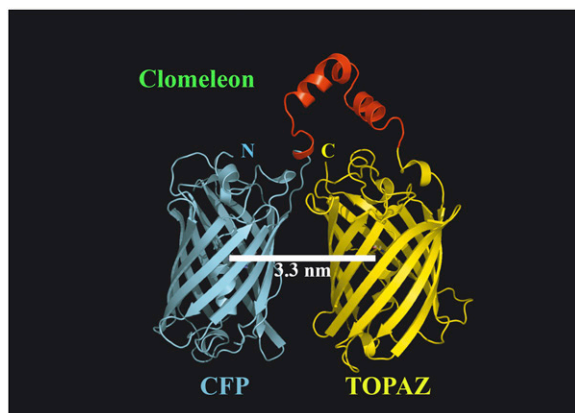

FIGURE 6   Molecular modeling of Clomeleon. The fluorescent domains, CFP (*cyan*) and Topaz (*yellow*) were set in parallel orientation since N- and C-terminal ends of either domain were on the same site. The intramolecular distance between CFP and Topaz chromophores was calculated to be 3.3 nm. A more compact antiparallel or crosslike orientation with distances close to 2.6 nm as found in homolog experimental structures sterically hindered the placement of the rTEV site containing linker without unfolding the adjacent helices of the fluorescent domains (data not shown).

of Clomeleon at this stage did not show a considerable difference from that of control ECFP (Fig. 7 b). DAS exhibited only positive values for the pre-exponential factors of all the lifetimes (Fig. 7 d). The fractional contributions of the multiple lifetimes did not show a significant change along the wavelength axis from the donor to the acceptor (Fig. 7 e). The lifetimes τ_1, τ_2, and τ_3 displayed contributions of $46 \pm 3\%$, $31 \pm 2\%$, and $24 \pm 1\%$ at the acceptor emission maximum, similar to the donor. Consequently, the mean lifetime at the donor emission peak of 1.86 ± 0.07 ns showed only minor changes up to 2.01 ± 0.08 ns at the acceptor emission maxima (Fig. 7 f).

At DIV 10, the majority of neurons were categorized into classes I and II with R-values of 0.47 ± 0.06 and 1.07 ± 0.08, respectively. The percentage of cells belonging to each of these classes were 58% and 33%, respectively ($N = 12$). Other classes with cells $<10\%$ of the total population were not considered in the classification. The fluorescence decay of Clomeleon at DIV 10 revealed similar lifetimes as DIV 7, but with the individual contributions of the lifetimes varying among the different classes (Table 2). At the donor emission maximum, τ_1 showed a significant decrease in its contribution from class I to II with a simultaneous increase of τ_3 for the same (Table 2). τ_2 displayed similar contributions for both the classes. Thus, the donor kinetics of Clomeleon in neurons belonging to class II revealed a shorter decay compared to control ECFP, in contrast to class I. DAS displayed negative values for the pre-exponential factors corresponding to τ_2 and τ_3 for class II in contrast to the unaffected positive values of class I. A reverse effect was observed at the acceptor emission maximum for class II, where τ_1 showed the maximum contribution of $87 \pm 7\%$ with the contributions of τ_2 and τ_3 being $<10\%$. For class I, the contribution of τ_1 decreased to $67 \pm 8\%$ with a corresponding increase in the contributions of τ_2 and τ_3 to $20 \pm 6\%$ and $14 \pm 5\%$ at the acceptor emission peak, respectively. Thus, for class II, the fractional contributions of the individual lifetimes revealed a drastic increase for τ_1 along the spectra with a simultaneous decrease for τ_2 and τ_3. Such a significant change was not observed for class I. This resulted in donor mean lifetimes of 2.00 ± 0.10 ns and 1.68 ± 0.04 ns (Table 2), which increased to 2.54 ± 0.21 ns and 3.08 ± 0.20 ns at the acceptor emission maxima, for classes I and II, respectively.

At DIV 14, neurons were divided into three classes with R-values of 0.65 ± 0.07, 1.03 ± 0.11, and 1.23 ± 0.04, where 40%, 40%, and 20% of the total population of cells belonged to classes I–III, respectively ($N = 10$). The multiple lifetimes of Clomeleon in this case were similar to those at DIV 7 and DIV 10 (Table 2). The contributions of the individual lifetimes at the donor emission maximum were similar to DIV 10 for classes I and II, whereas class III showed lower and higher contributions of τ_1 and τ_3, respectively (Table 2). Consequently, the donor fluorescence decays of classes II and III were shorter compared to class I as well as to control
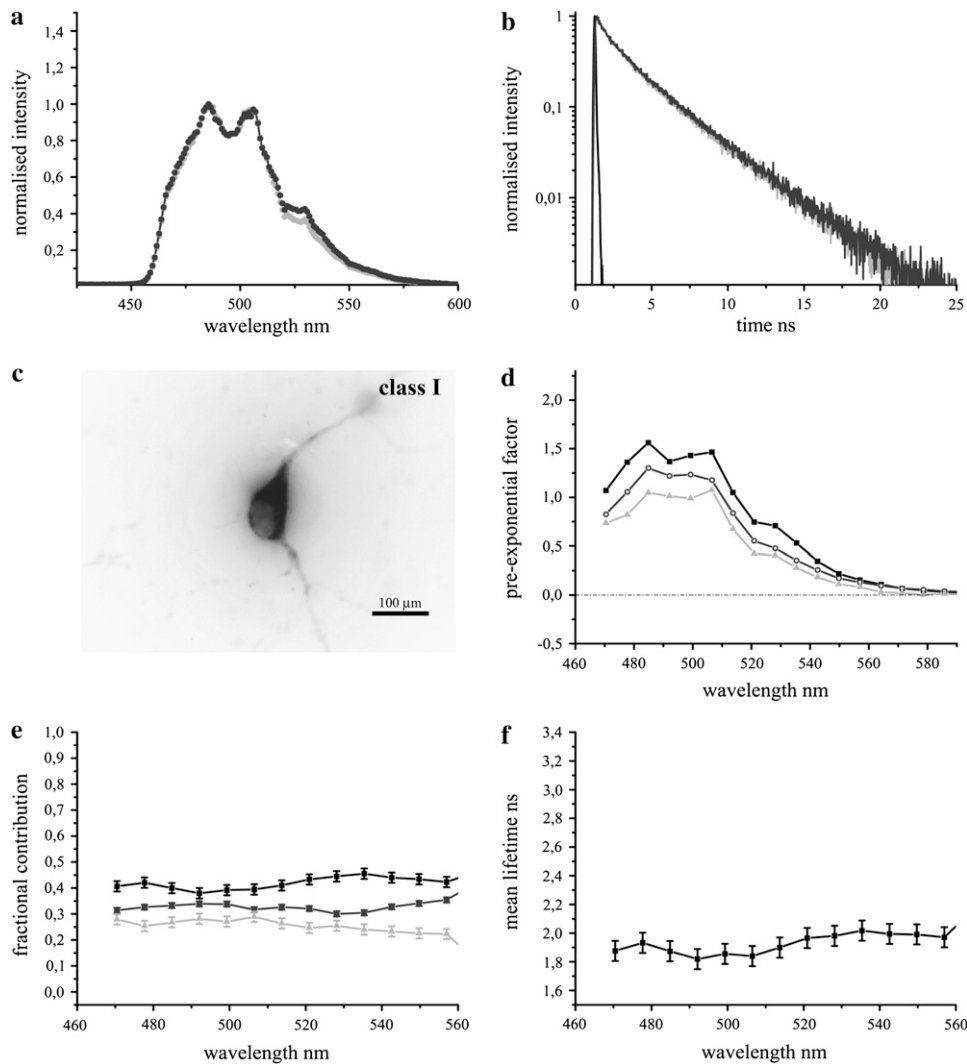
FIGURE 7 The fluorescence emission dynamics of Clomeleon at 420 nm excitation in hippocampal neurons at DIV 7. (*a*) Comparison of fluorescence emission spectra of ECFP (*light shading*) with Clomeleon (*shading*) at DIV 7. (*b*) Fluorescence decay of Clomeleon at the donor emission maximum at DIV 7 (*shading*) compared to ECFP (*light shading*). IRF is shown in solid representation. The fluorescence decay of Clomeleon was fit by a three-exponential model (Table 2). (*c*) A representative image of a neuron at DIV 7. (*d*) DAS of Clomeleon at DIV 7. The pre-exponential factors of τ_1 (*solid*), τ_2 (*shading*), and τ_3 (*light shading*) were positive similar to ECFP. (*e*) The contributions of the lifetimes τ_1 (*solid*), τ_2 (*shading*), and τ_3 (*light shading*) were calculated and plotted as normalized fractional contributions along the wavelength. (*f*) The mean lifetime of each emission band was plotted along the wavelength. The variability between the cells is shown by error bars. The mean lifetime of Clomeleon at the donor emission maximum was similar to that observed for ECFP.

ECFP (Fig. 8 *b*). DAS displayed negative values for the pre-exponential factors of τ_2 and τ_3 for classes II and III (Fig. 8 *e*), in contrast to class I (Fig. 8 *d*). The fractional contributions of τ_2 and τ_3 showed drastic decrease over the spectra with a simultaneous increase of τ_1 for these two classes. For classes II and III, at the acceptor emission peak, the major contributions were observed for τ_1 of $89 \pm 5\%$ and $84 \pm 1\%$, respectively, with τ_2 and τ_3 contributing $<10\%$. This was in contrast to class I where the corresponding contributions of τ_1, τ_2, and τ_3 were $64 \pm 7\%$, $21 \pm 3\%$, and $15 \pm 5\%$ at the acceptor emission maximum, respectively. As a result, the donor mean lifetimes for the classes I–III of 1.84 ± 0.15 ns, 1.73 ± 0.08 ns, and 1.57 ± 0.01 ns (Table 2), increased to 2.53 ± 0.19 ns, 3.08 ± 0.13 ns, and 2.96 ± 0.03 ns, respectively, at the acceptor emission maxima (Fig. 8 *f*).

At DIV 15, the percentage of cells belonging to class I was significantly reduced to $<10\%$ of the total population, whereas 50% and 40% of the total cells ($N = 10$) were divided into classes II and III with R-values of 1.05 ± 0.12 and $1.37 \pm$

0.07, respectively. The fluorescence decays, DAS and fractional contributions were similar to those observed at DIV 14.

Classification of neurons based on their R-values revealed a shift in their numbers from classes of low R-values to higher values drastically with neuronal maturation, thereby indicating that the majority of neurons expressing Clomeleon exhibited energy transfer when they were mature. At similar developmental stages of neurons, a reduction in the donor mean lifetimes was observed for classes I–III, whereas the acceptor mean lifetimes showed a corresponding increase for the same. An overall decrease in the donor mean lifetimes with a simultaneous increase in the acceptor mean lifetimes was also perceived with maturation.

Along with studying the developmental changes in the intracellular chloride concentrations, the differences in the ionic concentrations at different intracellular compartments were compared at the level of single cells. In mature neurons (DIV 15) expressing Clomeleon, different regions of interest (ROIs) in the same cell displayed differences in the acceptor
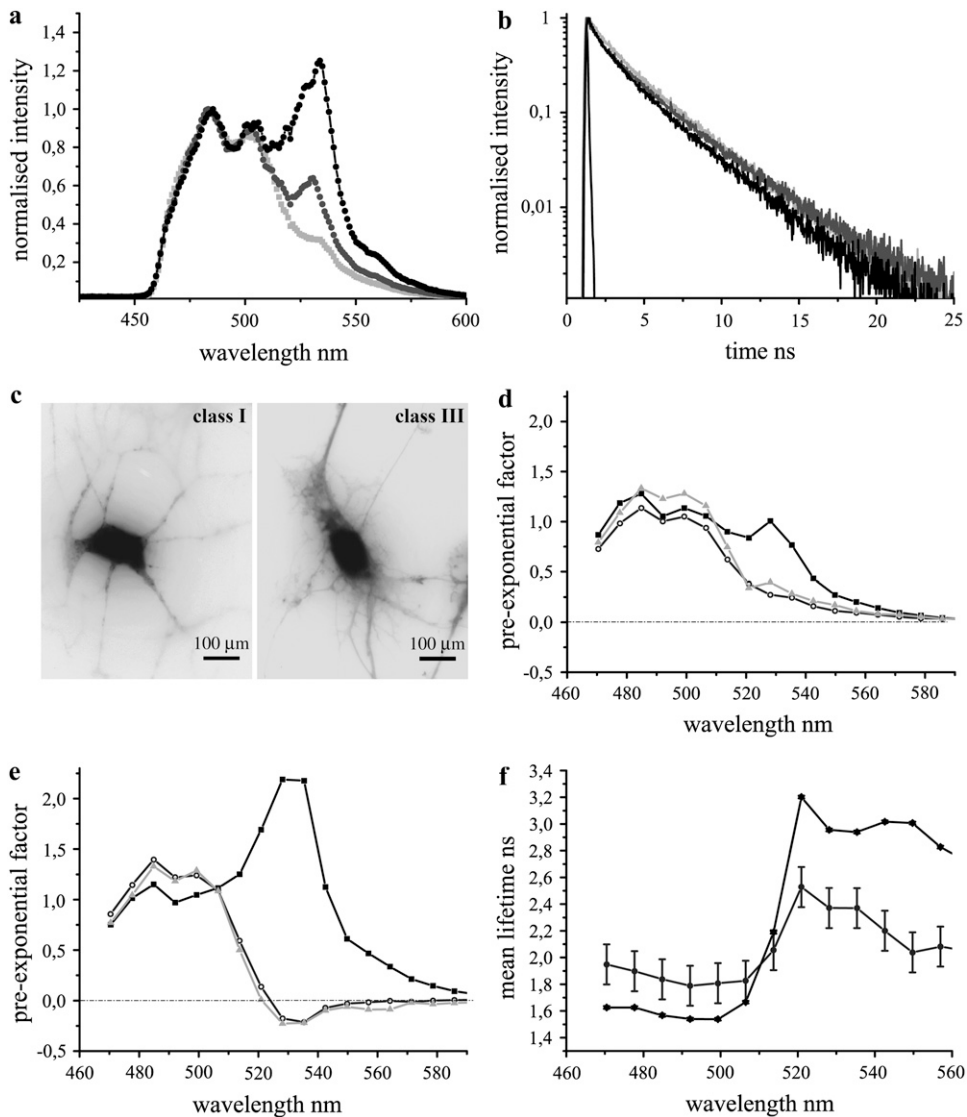
FIGURE 8 The fluorescence emission dynamics of Clomeleon at 420 nm excitation in hippocampal neurons at DIV 14. (*a*) Comparison of fluorescence emission spectra of ECFP (*light shading*) with Clomeleon of classes I (*shading*) and III (*dark shading*) with *R*-values of 0.65 ± 0.07 and 1.23 ± 0.04, respectively. (*b*) Fluorescence decays of Clomeleon at the donor emission maxima of classes I (*shading*) and III (*dark shading*) at DIV 14 compared to ECFP (*light shading*). IRF is shown in solid representation. The multiple lifetimes of Clomeleon at DIV 14 were similar to those observed at DIV 7, though for the majority of mature neurons at the donor emission maxima, the contribution of τ_3 increased with decreasing contribution of τ_1, in contrast to the latter (Table 2). (*c*) Representative images of neurons belonging to classes I and III at DIV 14. The neurons of class III were more developed compared to those of class I. (*d*) DAS of Clomeleon of class I. The pre-exponential factors of τ_1 (*solid*), τ_2 (*shading*), and τ_3 (*light shading*) were positive similar to ECFP. (*e*) DAS of Clomeleon of class III. The pre-exponential factors of τ_2 (*shading*) and τ_3 (*light shading*) displayed negative values in contrast to class I. (*f*) Mean lifetimes of each emission band of classes I and III were plotted along the wavelength. The variability between the cells is shown by error bars. For class III (*solid*), the variability was lower compared to class I (*shading*).

dynamics (Fig. 9, *a* and *b*). A better rise was observed at ROIs close to the periphery of the cell compared to the cell center, indicating better FRET for Clomeleon at the former. A confirmation of this was done using TIRF, which illuminated only the fluorophores close to the cell periphery.

The lifetimes of Clomeleon by epifluorescence and TIRF excitations were 3.19 ± 0.01 ns (τ_1), 1.36 ± 0.03 ns (τ_2), and 0.34 ± 0.04 ns (τ_3). In the TIRF mode, τ_3 exhibited negative pre-exponential factors (<5%) in the acceptor channel. In the donor channel, τ_1, τ_2, and τ_3 displayed similar contributions

TABLE 2 Fluorescence emission dynamics of Clomeleon at different stages of hippocampal neuronal development

Cell	DIV	N(%)	Class	R	τ_1 (ns)	τ_1 (%)	τ_2 (ns)	τ_2 (%)	τ_3 (ns)	τ_3 (%)	τ_{mean} (ns)
Neurons	7		I	0.42 ± 0.04	3.39 ± 0.05	40 ± 2	1.35 ± 0.06	33 ± 1	0.26 ± 0.03	27 ± 2	1.86 ± 0.07
	10	58	I	0.47 ± 0.06	3.37 ± 0.06	45 ± 3	1.38 ± 0.13	32 ± 3	0.24 ± 0.10	23 ± 2	2 ± 0.10
	10	33	II	1.07 ± 0.08		34 ± 1		33 ± 2		33 ± 2	1.68 ± 0.04
	14	40	I	0.65 ± 0.07	3.42 ± 0.05	39 ± 4	1.36 ± 0.07	32 ± 2	0.22 ± 0.05	29 ± 5	1.84 ± 0.15
	14	40	II	1.03 ± 0.11		35 ± 2		35 ± 2		31 ± 2	1.73 ± 0.08
	14	20	III	1.23 ± 0.04		30 ± 1		34 ± 2		35 ± 2	1.57 ± 0.01
COS-7				1.05 ± 0.18	3.40 ± 0.02	32 ± 2	1.32 ± 0.05	36 ± 1	0.17 ± 0.01	32 ± 2	1.61 ± 0.06

The lifetimes of Clomeleon were consistent along development, though a difference in the contributions of the individual lifetimes was observed. The percentage of the total population of cells in each class is shown (*N%*). The percentage of contributions of τ_1, τ_2, and τ_3 are denoted as τ_1%, τ_2%, and τ_3%, respectively. The mean lifetimes for the respective classes at each stage are denoted as τ_{mean}. Comparison of lifetimes and contributions obtained from COS-7 cells showed that they were similar to class III at DIV 14.
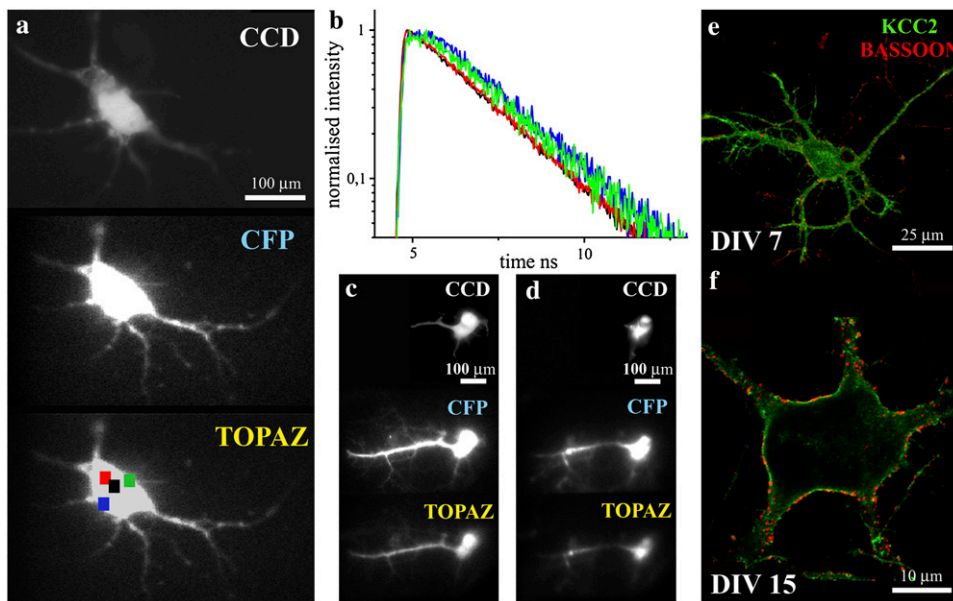
FIGURE 9 Mature neurons (DIV 15) expressing Clomeleon as observed in the imaging detector. (*a*) The fluorescence emission was split up into CFP and Topaz emission bands as shown. A comparison with the corresponding fluorescence image from the CCD was done (*top*). Selected ROIs are shown as colored squares. (*b*) Analysis of the differential acceptor rise at different intracellular regions of a cell. A better rise in the acceptor dynamics was observed at the cell periphery (*green*, *blue*) compared to the cell center (*black*, *red*). Comparison of cells in epifluorescence (*c*) and TIRF modes (*d*). Negative values for the pre-exponential factors of τ_3 were observed in the acceptor channel in the TIRF mode. Immunostainings against KCC2 (*green*) and Bassoon (*red*) were done to compare the maturity of cells at DIV 7 (*e*) and DIV 15 (*f*). At DIV 7, a random intracellular staining of low amounts of KCC2 was observed in contrast to that observed at DIV 15, where the majority of cells showed a clear membrane staining with enrichment of KCC2 at specific regions of the cell membrane. The synapses marked by Bassoon increased at DIV 15 (*f*), compared to DIV 7 (*e*).

in both the illumination modes of $31 \pm 2\%$, $37 \pm 1\%$, and $33 \pm 1\%$, respectively. In the acceptor channel, similar to that observed with the point detector, τ_1 showed the maximum contribution of 86% in the epifluorescence mode, which increased to 94% in the TIRF mode. The contributions of τ_2 and τ_3 also decreased in the TIRF mode, although they were individually below 10%. Consequently, an increase in the acceptor mean lifetime from 2.88 ns to 3.10 ns was observed on changing from the epifluorescence to the TIRF mode (Fig. 9, *c* and *d*).

The chloride transporter KCC2 shows an upregulation with neuronal development, whose expression pattern has also been functionally linked with the shift of GABA-mediated responses from depolarizing to hyperpolarizing (8). Immunostainings against KCC2 and the presynaptic marker protein Bassoon was done for comparing the maturity of the cells at individual stages (Fig. 9, *e* and *f*). At DIV 7, a random intracellular staining of low amounts of KCC2 was observed (Fig. 9 *e*) in contrast to those at DIV 15, where the majority of cells showed a clear membrane staining with enrichment of KCC2 at specific regions of the cell membrane (Fig. 9 *f*). The synapses marked by Bassoon also increased at DIV 15 compared to young neurons (Fig. 9, *e* and *f*). The synaptic contacts were observed between KCC2-enriched regions, indicated by the synapses shown by the presynaptic marker Bassoon. This was in agreement with the previous reports where a higher expression of KCC2 was seen at the vicinity

of excitatory inputs in the hippocampus, possibly in close association with extrasynaptic GABA$_A$ receptors (25).

Overall changes in the fluorescence spectra, lifetimes as well as in the contributions of individual lifetimes of Clomeleon were observed with development (Figs. 7–9). Mature neurons expressing Clomeleon revealed higher FRET efficiencies in contrast to young cells.

Effect of neuronal development on the energy transfer dynamics of Cameleon

To study the effects of intracellular ionic concentrations on FRET for an independent construct with a less sensitive acceptor, Yellow Cameleon YC2.3 was monitored at different developmental stages (DIV 7, 10, 15) of hippocampal neurons (data not shown). Cameleon consisted of tandem fusions of ECFP and a photostable YFP variant Citrine. Binding of Ca^{2+} to Cameleon increased the efficiency of energy transfer between the flanking GFPs (26). YC2.3 exhibited the fluorescence emission maximum for ECFP at 486 nm and for Citrine at 529 nm. At DIV 7, the total cell population was divided into two with *R*-values of 1.04 ± 0.12 and 1.55 ± 0.27. The fluorescence decay was fit by a three-exponential model with lifetime components of 3.26 ± 0.1 ns (τ_1), 1.39 ± 0.14 ns (τ_2), and 0.3 ± 0.07 ns (τ_3). The multiple lifetimes of Cameleon were in good agreement with the previous reports in solutions (27). DAS showed negative

values for the pre-exponential factors of τ_2 and τ_3. τ_1 displayed a significant increase in its contribution with increasing wavelength, with a corresponding decrease for the short lifetime components. At DIV 10, R-values similar to DIV 7 were observed. At DIV 15, R-values of YC2.3 were reduced to 0.65 ± 0.02. The fluorescence decay in this case was also fit by a three-exponential model with lifetime components similar to the previous cases. No negative DAS was detected for any of the lifetimes at this stage.

Cameleon showed FRET in young neurons where the intracellular calcium concentrations are high, in contrast to mature neurons.

3. The suitability of Clomeleon as a ratiometric and lifetime indicator along development of living neurons was ensured by independent methods. Ratiometric studies using chloride-regulated COS-7 cells and lifetime measurements on purified solutions of Clomeleon were performed for the purpose.

Fluorescence dynamics of Clomeleon on regulating chloride concentrations

COS-7 cells expressing Clomeleon exhibited R-values of 1.05 ± 0.18. The fluorescence decay in this case was fit with three lifetimes of 3.40 ± 0.02 ns, 1.32 ± 0.05 ns, and 0.17 ± 0.01 ns showing comparable contributions at the donor emission maximum ($N = 5$, Table 2). At the acceptor emission peak, the maximum contribution was observed for τ_1 of $88 \pm 2\%$ with τ_2 and τ_3 contributing $<10\%$. This resulted in an increase in the mean lifetime of Clomeleon from 1.61 ± 0.06 ns to 3.10 ± 0.08 ns along the spectra, from the donor to the acceptor emission maxima.

COS-7 cells were clamped to three different chloride concentrations of 0 mM, 30 mM, and 50 mM maintaining the pH constant at 7.4, and the individual R-values were calculated (Fig. 10 a). Cells at 0 mM Cl$^-$ yielded R-values of 1.59 ± 0.18, which was reduced with increasing chloride concentrations to 1.07 ± 0.14 and 0.58 ± 0.07 at 30 mM and 50 mM Cl$^-$, respectively. Since the major influences on the Clomeleon fluorescence including chloride and pH were controlled using Tributyltin chloride (TBTC) and Nigericin, respectively, the changes in R-values were concluded to be due to chloride changes. Comparison of R-values from externally regulated COS-7 cells with those from hippocampal neurons yielded the intracellular chloride concentrations at different stages of maturation. A significant decrease in chloride concentrations along neuronal development was observed (Fig. 10 b). The young neurons at DIV 7 showed intracellular chloride concentrations of 58 ± 3 mM. At DIV 10, classes I and II revealed chloride concentrations of 56 ± 3 mM and 26 ± 4 mM, respectively, whereas mature cells of class III at DIV 14 and 15 exhibited chloride concentrations
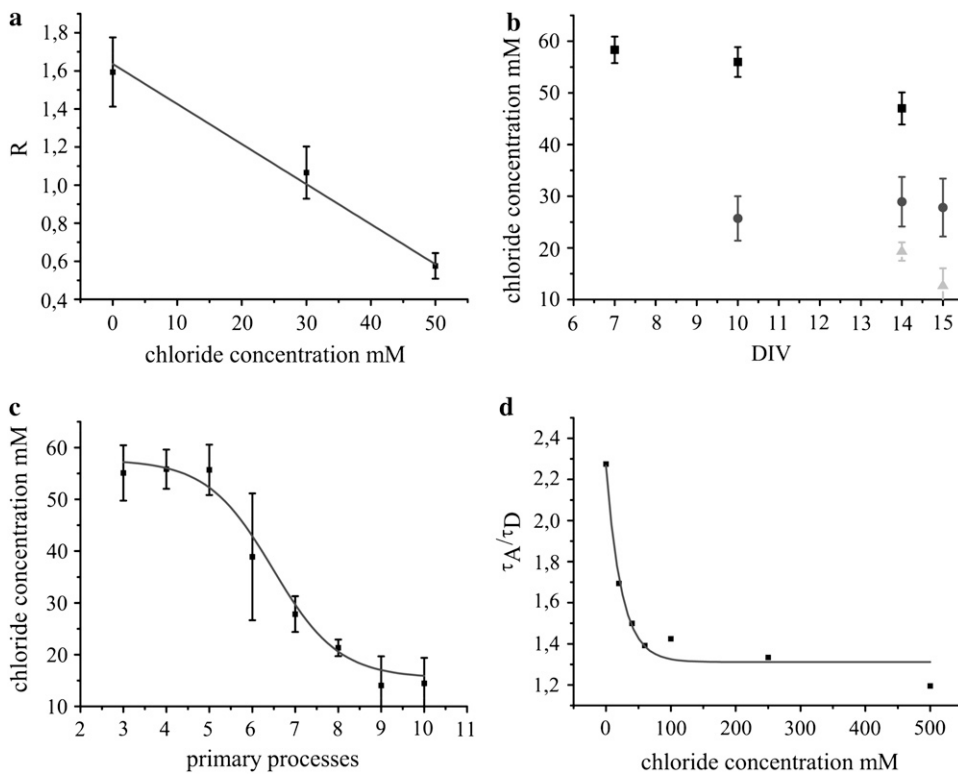

FIGURE 10 (a) The R-values of COS-7 cells expressing Clomeleon clamped to 0 mM, 30 mM, and 50 mM chloride concentrations. The R-values decreased with increasing chloride concentrations from 1.59 ± 0.18 (0 mM) to 0.58 ± 0.07 (50 mM). (b) Comparison of R-values from COS-7 cells yielded the intracellular chloride concentrations in hippocampal neurons at different stages of maturation. A drastic decrease in the chloride concentrations was found for all the classes along neuronal development. The minimum chloride concentration was observed for class III (*light shading*) at DIV 15 and the maximum for class I (*solid*) at DIV 7. (c) A sigmoidal decrease in the intracellular chloride concentrations of neurons with increasing maturation was observed on comparing the individual R-values with the number of primary processes they possess. (d) The ratios of acceptor-to-donor mean lifetimes of Clomeleon in solution at varying chloride concentrations. A comparison of these ratios from solutions with those obtained from the different fractions of mature neurons allowed the determination of intracellular chloride concentrations of the latter, similar to those obtained from R-values of COS-7 cells.

of 19 ± 2 mM and 13 ± 3 mM, respectively. The calculated results were in agreement with electrophysiological reports on overall changes of chloride during neuronal development (10).

The dependence of the fluorescence properties of Clomeleon on maturation of neurons was further confirmed by comparing the R-values of individual cells with the number of primary processes they possess. An overall increase in R-values or higher FRET was observed for the cells showing higher number of processes and branching, or cells that were more developed. Comparison of the results with COS-7 cells revealed a sigmoidal decrease in the intracellular chloride concentration of individual cells with the degree of maturation (Fig. 10 c). Similar number of processes (e.g., six) gave higher and lower chloride values at young and mature stages, respectively, thereby accounting for the high deviation observed.

The multiexponential analysis of chloride-clamped COS-7 cells could not be performed due to the presence of a short lifetime component (<10 ps) arising from TBTC in gluconate buffer. Using the lifetimes obtained from purified Clomeleon on varying the chloride concentrations, the ratios of acceptor/donor mean lifetimes were calculated (Fig. 10 d). Comparing these values with those from neurons at different stages of maturation, the individual chloride concentrations for the different fractions of mature neurons (DIV 15) were calculated to be 61 ± 14 mM, 18 ± 5 mM, and 14 ± 1 mM for classes I–III, respectively. Since the majority of young neurons show low pH levels (28) which influence CFP and Topaz differentially (29), comparable measurements could not be done in young stages.

Clomeleon was used successfully as a ratiometric and lifetime indicator, whose biophysical properties were used for studying the changes in the intracellular chloride concentrations during neuronal maturation.

DISCUSSION

Fluorescence properties of CFP in solution and in living neurons

Although there was no shift in the fluorescence emission maximum of CFP on varying the pH levels, an increase in the contribution of its red-shifted shoulder at 505 nm was observed on lowering the pH (Fig. 2 a). The quenching effects on intensity of GFPs due to acidification have already been reported (29), although their effect on lifetimes has not yet been deeply investigated. Acidic pH levels resulted in a significant (20%) third lifetime component of 0.28 ns (τ_3), in addition to the typical biexponential decay of CFP (30), which shortened its overall fluorescence decay (Fig. 2 b). The DAS of CFP also confirmed the source of the third lifetime to be the CFP chromophore, with the spectral spread of the pre-exponential factors of all the lifetimes being similar. The plot of fractional contributions of CFP revealed significant quenching of τ_1 at acidic pH levels, whereas τ_2

remained unaffected (Fig. 2 c). The relatively chloride-insensitive CFP showed only minimal effects on increasing the chloride in solution. The small shift in the donor mean lifetimes of CFP on varying the chloride concentrations could be well expected due to the minor variations in the buffer pH levels.

The biexponential decay of CFP with lifetimes of 3.26 ± 0.10 ns (τ_1) and 1.12 ± 0.03 ns (τ_2) were changed to 3.09 ± 0.09 ns, 1.38 ± 0.08 ns, and 0.28 ± 0.06 ns (τ_3) at acidic pH levels. According to our kinetic model of CFP, the unperturbed τ_1 of CFP (3.3 ns) and the first emission maxima originates from its first conformation, whereas the unperturbed τ_2 (1.1 ns) of CFP as well as the second emission peak arises from its second conformation (31). It could be assumed that the individual conformations of CFP take part in quenching independently (32). There are different amino-acid residues in CFP, which could account for its complex pH sensitivity (33). From the effects observed in solution at 0 mM Cl$^-$, the first conformation of CFP was concluded to be most affected by quenching at acidic pH levels. Such a difference in quenching effects for the two lifetimes could arise only if the folding of the second conformation of CFP is in such a way as to introduce a steric shielding for the respective amino acid residues from the quenchers. This model was also in agreement with the deviations in the emission spectra of CFP at 0 mM Cl$^-$ at varying pH levels. Lesser quenching of the first conformation of CFP was revealed at higher pH levels, resulting in a higher ratio for the major peak of CFP at 486 nm compared to its shoulder. However, if the quenching of τ_1 of CFP (3.3 ns) would result in lifetimes close to the unperturbed τ_2 of CFP (1.1 ns) as displayed at low pH levels, this would in turn reduce the quenching effects observed for the resulting lifetime (1.38 ns) due to the contribution of unquenched τ_2.

In young hippocampal neurons, ECFP displayed a three-exponential fluorescence decay, in contrast to its typical biexponential nature, with similar contributions for all the lifetimes (Table 1). The presence of the third lifetime component was not observed in the major fraction of neurons at DIV 15, resulting in an overall increase in the mean lifetime of ECFP along neuronal development. In all the cases, where the fluorescence decay of ECFP was two- or three-exponential, the pre-exponential factors of all individual lifetimes were positive (Fig. 3, c and d). The source of the short lifetime component of 0.29 ns for CFP in young neurons could be explained by the difference in the pH levels of the cells, which shows a shift with maturation (28). The multiple lifetimes in neurons were similar to those observed in solution at different pH levels. This was also corroborative with the deviations in the emission spectra of ECFP on varying the pH.

A comparison of our results with the previous reports (28) showed a developmental shift of pH and chloride in different fractions of neurons. This could in turn indicate overlapping

fractions, as observed from our results in cells and solution. The differences in the fluorescence dynamics of ECFP observed with neuronal development due to effects like quenching have to be taken into account when studying interactions in living cells, since the reduced donor mean lifetimes or the presence of a third lifetime component could be misinterpreted as the presence of energy transfer.

Fluorescence dynamics of Clomeleon in solution

Quenching effects were observed for purified Clomeleon on increasing the chloride concentrations. At 0 mM Cl^-, only the shortest lifetime component (τ_3) displayed negative pre-exponential factors in contrast to the other chloride concentrations, where both the short lifetime components (τ_2 and τ_3) were involved in FRET. This would indicate an involvement of both conformers of CFP in energy transfer, probably displaying different quenching patterns (31). The lifetimes τ_1 and τ_3 showed drastic increase and decrease in their contributions on increasing the chloride levels, resulting in an overall increase in the donor mean lifetimes (Fig. 4, b and c). The slight reduction in the contribution of τ_2 showed that it was not unaffected (Fig. 4 b). In the acceptor channels, the drastic decrease in the contribution of τ_1 indicated significant quenching of Topaz on increasing the chloride concentrations. Consequently, the mean lifetimes of Clomeleon in the acceptor channels were observed to approach mean lifetimes of CFP at high chloride concentrations.

The high quenching effect of Topaz could be explained by its static quenching due to the possibility of its direct binding to chloride ions (10). In this case, bound or contact quencher complexes would be present in the ground state, which competes with the ground state of Topaz for incident excitation. This would in turn yield excited acceptor-quencher complexes whose excitation results in instantaneous quenching on absorption (34). This was also in agreement with the observation that Clomeleon at high chloride concentrations, on direct excitation for steady-state imaging, showed reduced fluorescence with the YFP filter. Also, no additional lifetimes were observed in the acceptor channels on increasing the chloride concentrations. Further, the chloride association from the bulk solution might favor protonation and thereby reduce the fluorescence of Topaz (32). The high static quenching of Topaz would override the possibility for Clomeleon to show FRET. Depending on the prevalent effects, the overall fluorescence properties of Clomeleon was altered. The lifetimes of Clomeleon remained unchanged in presence of high quenching effects too, since no conformational change was involved.

The pH effects on the fluorescence emission spectra of Clomeleon were significant. At 0 mM Cl^-, R-values decreased to <50% at acidic pH levels (Fig. 4 d). The fluorescence lifetimes of Clomeleon approached those of CFP at low pH levels. The fractional contributions of τ_3 were higher at pH levels <6.5 and >7.2 due to the different excited state reactions involved. A reverse effect with decreased contribution of τ_1 was observed for the same, whereas τ_2 remained relatively unaffected (Fig. 4 e). At low pH levels, Clomeleon exhibited high quenching effects similar to CFP, whereas at high pH levels FRET was significant. As a result, a Gaussian distribution was observed for the donor mean lifetimes at approximately pH 6.8 (Fig. 4 f).

For the protease-digested Clomeleon, there was no Topaz enhancement due to lack of FRET and very low direct excitation (Fig. 5 a). The change of the resulting fluorescence decay from three to two exponentials with similar lifetimes of CFP also confirmed the absence of any undigested sample (Fig. 5, b, d, and e). Consequently, the mean lifetimes of digested Clomeleon were similar to CFP alone (Fig. 5 f). The unperturbed kinetics of the digested sample under varying chloride concentrations and pH levels also excluded the possibility of any additional lifetimes in the acceptor channels arising due to quenching effects of Topaz, as expected.

The observation of negative amplitudes for τ_2 and τ_3 of Clomeleon at chloride concentrations (>0 mM) indicated the participation of both conformations of CFP in FRET. Since it was not possible to discriminate which among the CFP conformers was the source of the shortest FRET lifetime (τ_{DA}), distance calculations were done using both probabilities. Assuming that the FRET lifetime of 0.21 ns arises from the quenching of the second conformation of CFP (1.1 ns), such a calculation yielded the efficiency to be 80% and consequently the distance d to be 39 Å. Distance calculations using conventional mean lifetimes were not possible due to the presence of free CFP conformers not involved in energy transfer. The fluorescence characteristics of both CFP and Topaz were perturbed due to pH effects. Further, the changes in the absorption spectra of Topaz due to the binding of chloride ions would influence the d_0 values. Therefore, the distance determination of Clomeleon was performed only at 0 mM Cl^- at pH 7.4.

τ_1 of Clomeleon can be taken as the unperturbed donor lifetime, which is not involved in any excited state reaction. This can be considered as the subpopulation of one of the CFP conformers that are unquenched. Calculation of mean lifetimes of Clomeleon excluding this contribution of free conformers yielded $\tau_{DA} = 0.57$ ns. Using τ_{mean} of CFP under similar conditions (0 mM Cl^-, pH 7.4) as τ_D, FRET efficiency of Clomeleon was calculated to be 76.5%, which in turn yielded $d = 40$ Å, close to the values calculated from the individual lifetimes of the assumed model (39 Å). The slight increase in this value could be explained by the presence of the second set of unquenched conformers of CFP (giving rise to the unperturbed lifetime τ_2), whose resolution is much more complicated. According to the previous assumption, this lifetime would be close to the quenched lifetime from τ_1, beyond the discriminating capability of any currently used multiexponential analysis methods.

However, the degree of competition between FRET and quenching of CFP can be understood by comparing the

dynamics of purified CFP and Clomeleon under varying pH conditions. It was observed that the quenching of CFP at pH 7.0 resulted in a reduction of its mean lifetime to 2.23 ns (0 mM Cl$^-$, Fig. 2 d), whereas in the presence of FRET at the same conditions, this was reduced to 1.43 ns (Fig. 4 f). Therefore the presence of energy transfer significantly affected the fluorescence dynamics of CFP compared to the quenching by acidic pH levels, as expected. The unperturbed mean lifetime of CFP at pH 8.0 was observed to be 2.5 ns (Fig. 2 d). The FRET efficiency of Clomeleon was calculated with the unperturbed as well as the quenched lifetimes of CFP at different pH levels, which yielded 43% and 36%, respectively. The difference of 7% indicated the efficiency of excited state reactions of CFP excluding FRET. The quenching effects on CFP excluding FRET increased from 0% to 18% on lowering the pH from 8.0 to 6.0, whereas the FRET efficiency of Clomeleon decreased from 64% to 38% in similar conditions.

The differential effects on Clomeleon under varying conditions revealed that the quenching effects as well as energy transfer for the two conformations of CFP could be independent from each other.

Fluorescence dynamics of Clomeleon along neuronal development

The multiple lifetimes of Clomeleon were constant throughout development, indicating that no conformational change was involved (Table 2). The contributions of the individual lifetimes and their spectral spread showed clear differences along development (Table 2, Figs. 7 and 8), thereby resulting in an overall decrease and a simultaneous increase in the mean lifetimes at the donor and acceptor emission maxima with maturation (Figs. 7 f and 8 f). The pre-exponential factors of the individual lifetimes showed only positive values for all cells at DIV 7 (Fig. 7 d) similar to ECFP, whereas the contributions of τ_2 and τ_3 showed negative values for the majority of mature neurons (Fig. 8 e). Such a change in sign or negative amplitudes for the lifetimes at the acceptor peak could only arise due to the presence of energy transfer (22). The fractional contributions of individual lifetimes also differed between cells showing high FRET efficiency from those which do not. In the former, the contribution of τ_1 increased drastically along the wavelength axis combined with a simultaneous decrease of τ_2 and τ_3, whereas in the latter, no such change was observed (Fig. 7 e).

For the mature neurons, fluorescence lifetime analysis revealed higher FRET with negative values for the pre-exponential factors of τ_3 at the cell periphery, as indicated by TIRF studies. The higher expression of the potassium chloride cotransporter KCC2 at the cell periphery compared to the cell center could explain the lower chloride concentrations at the former (Fig. 9). In the imaging detector, negative pre-exponential factors were observed only for τ_3, in contrast to the measurements from the point detector. This could be accounted by the lack of wavelength resolution in the imaging detector due to the usage of bandpass filters for collecting the donor and the acceptor fluorescence, with unavoidable cross talk between the channels. Though the influence of pH on lifetimes cannot be avoided, negative amplitudes for the multiexponential components at the acceptor emission maximum would arise only in presence of FRET.

The classification of neurons in the present work was based on the R-values of individual cells. The subpopulations of cells, namely the presence of excitatory (pyramidal) and inhibitory (interneurons) neurons, were not individually considered. Since both these groups exhibit high intracellular chloride concentrations at young stages that lower on maturation, the majority of neurons were expected to belong to class I at DIV 7, which shifted to classes II and III with maturation (DIV 14 and 15). Further, in dissociated hippocampal cultures, <20% of interneurons were expected. The fraction of neurons showing high chloride concentrations or low R-values in mature stages could in turn denote those cells where GABA remained excitatory. Since no deviation was observed in the measured results from those expected, further classifications were not considered for a detailed study.

The fluorescence decay of Clomeleon measured in COS-7 cells (pH 7.4) yielded lifetimes similar to those observed in neurons with the contributions and mean lifetimes similar to the class showing highest R-values at DIV 14 or the lowest intracellular chloride concentrations (Table 2). This was also in agreement with the measurements of ECFP in COS-7 cells where the mean lifetimes were similar to those observed for the majority of mature neurons, indicating similar chloride and pH levels for both (Table 1). The intracellular chloride concentrations calculated using chloride-regulated COS-7 cells were in agreement with the previous reports on overall changes of chloride during neuronal development (10).

Since the donor CFP itself shows heterogeneity in its lifetimes along development of neurons, a direct calculation of FRET efficiency or chloride determination from the absolute donor or acceptor lifetimes can be misleading. In this regard, chloride calculations from ratiometric parameters like R are better conceivable, since they average-out these different effects to a good extent and will be, thereby, less affected. Utilizing this possibility, the ratios of acceptor/donor mean lifetimes were calculated from purified Clomeleon at pH 7.4 under varying chloride conditions and compared with those obtained from the different fractions of neurons at a particular maturation stage, namely DIV 15. According to previous reports, though heterogeneity in pH levels between individual neurons is to be expected, the majority of cells at this stage would exhibit pH levels close to 7.4 and thereby be comparable (28). This in turn resulted in similar values of intracellular chloride concentrations from the ratio of lifetimes with those calculated from R-values, namely 61 ± 14 mM and 56 ± 3 mM for class I and 14 ± 1 mM and 13 ± 3 mM for class III, respectively. In the minor

fraction of mature neurons of class I, FRET was hindered due to high intracellular chloride concentrations as well as due to low pH levels, accounting for the high deviations observed. Since the lifetimes obtained from neurons were not measured under regulated conditions, more precise calculations were not possible because of the differential influences of pH on CFP and Topaz.

Thus Clomeleon was used for the first time as a ratiometric lifetime indicator for chloride, which was successful under comparable pH conditions. Usage of pH-insensitive probes in the ratiometric biosensors would make such direct calculations of intracellular ionic concentrations of cells more feasible.

Kinetic model for simultaneous quenching and FRET in Clomeleon

The fluorescence dynamics of Clomeleon and Cameleon were studied simultaneously to understand the mechanism of how energy transfer occurs in presence of quenching effects of the solvent. Strong quenching effects were observed for Clomeleon at high chloride concentrations as well as at low pH levels. In Clomeleon, the presence of these two quenching effects overrode the possibility for energy transfer, though CFP and Topaz were well within the FRET distance. The fluorescence dynamics of Cameleon in young neurons showed that even in presence of quenching effects due to high anionic concentrations and low pH levels, FRET could be observed. This would indicate that even in presence of quenching, energy transfer was possible from the donor molecule. Thus the possibility to observe FRET would purely depend on the sensitivity of the acceptor to the ionic effects. This was very well the case of Cameleon where Citrine is expected to be more stable as well as less sensitive to ions compared to Topaz. This would further confirm that the biophysical properties of Clomeleon depend on the properties of Topaz alone and not on CFP, though the quenching effects were observed for the latter too, making it an ideal optical indicator for ratiometric studies inside a living cell.

The present approach of studying the multiple components of fluorescence decays and their contributions of both donor and acceptor molecules made it possible to discriminate energy transfer mechanisms from other excited state reactions, which is not possible by conventional FRET-FLIM methods. Further, information concerning the sources of the different lifetimes, as well as the mechanisms affecting them individually, was obtained to a large extent. Thus, with the current work, it was possible to arrive at a model, which could explain the mechanism of how competitive quenching effects as well as excited state reactions present in a single molecule could affect its biophysical properties. Further, the deviations in the fluorescence dynamics of the popular fluorescent probe ECFP due to ionic effects have been thoroughly discussed, which could play a major role in the interpretations of results in the current field of work.

In the case of Clomeleon where the donor and acceptor fluorophores are in a single molecule and within the Förster radius, 1:1 stoichiometry was achieved, thereby allowing us to study FRET. For interaction studies of fusion proteins expressed in cells, this may not be the case since the fraction of interacting molecules may be low, thereby reducing the probability of FRET determination by measuring negative DAS. Still, a reduction in DAS at the acceptor emission maximum as well as changes in the fractional contributions could be expected for the participating lifetimes, thereby asserting the importance of studying the multiple lifetimes of donor and acceptor molecules in addition to the conventional way of monitoring only the donor mean lifetimes, which could be influenced by other cellular effects like pH, as discussed previously.

CONCLUSIONS

A combination of FRET-FLIM techniques along with single photon counting was used to study the fluorescence dynamics of ECFP as well as of the ratiometric chloride indicator Clomeleon along development of hippocampal neurons.

DAS of ECFP in young neurons as well as at acidic pH levels revealed three lifetime components in the multiexponential analysis to be originating from the ECFP chromophore itself. Based on these results, a model was suggested on how differential quenching of the two conformers of ECFP could take place. These kinds of cellular effects, which cause deviation in the fluorescence properties of probes, have to be taken into account when studying interactions in living cells, since a reduction in the donor mean lifetimes or the presence of additional lifetime components could be misinterpreted as presence of energy transfer. Interestingly, the fluorescence dynamics of ECFP was unaffected by other high ionic influences, making it a good pH indicator in living neurons.

Clomeleon was used as an optical indicator for monitoring the intracellular chloride concentrations in living cells by steady-state and time-resolved spectroscopy. Confirmation of the intracellular chloride concentrations of neurons at different developmental stages was done by independent methods. A direct correlation of FRET in Clomeleon with the overall development of individual neurons as well as at different subcellular compartments was also possible. Clomeleon was used both as a conventional ratiometric indicator and as a lifetime indicator. The latter was successful in obtaining a direct readout of intracellular chloride concentrations in neurons where pH levels were high. Since neurons show a developmental shift of pH with maturation that influences both CFP and Topaz differentially, the feasibility of this new approach was limited only to mature neurons.

In presence of the different challenges posed in studying FRET by FLIM in living neurons, study of DAS with simultaneous donor and acceptor analysis was necessary to discriminate the presence of energy transfer from other photophysical processes. The results helped to arrive at a

kinetic model for the mechanism when competitive quenching effects as well as energy transfer simultaneously occur in the same molecule. The usage of photostable donors like Cerulean (35) and pH-insensitive mutants of Sapphire (36) may improve the range of applications where biosensors could be used as ratiometric indicators in living neurons.

REFERENCES

1. Hink, M. A., T. Bisselin, and A. J. Visser. 2002. Imaging protein-protein interactions in living cells. *Plant Mol. Biol.* 50:871–883.

2. Chan, F. K., R. M. Siegel, D. Zacharias, R. Swofford, K. L. Holmes, R. Y. Tsien, and M. J. Lenardo. 2001. Fluorescence resonance energy transfer analysis of cell surface receptor interactions and signaling using spectral variants of the green fluorescent protein. *Cytometry.* 44: 361–368.

3. Harpur, A. G., F. S. Wouters, and P. I. Bastiaens. 2001. Imaging FRET between spectrally similar GFP molecules in single cells. *Nat. Biotechnol.* 19:167–169.

4. Sanders, R., A. Draaijer, H. C. Gerritsen, P. M. Houpt, and Y. K. Levine. 1995. Quantitative pH imaging in cells using confocal fluorescence lifetime microscopy. *Anal. Biochem.* 227:302–308.

5. Chen, Y., J. D. Mills, and A. Periasamy. 2003. Protein localization in living cells and tissues using FRET and FLIM. *Differentiation.* 71:528–541.

6. Tramier, M., I. Gautier, T. Piolot, S. Ravalet, K. Kemnitz, J. Coppey, C. Durieux, V. Mignotte, and M. Coppey-Moisan. 2002. Picosecond-hetero-FRET microscopy to probe protein-protein interactions in live cells. *Biophys. J.* 83:3570–3577.

7. Loefroth, J. E. 1986. Time-resolved emission spectra, decay-associated spectra and species-associated spectra. *J. Phys. Chem.* 90:1160–1168.

8. Ben-Ari, Y. 2002. Excitatory actions of GABA during development: the nature of the nurture. *Nat. Rev. Neurosci.* 3:728–739.

9. Griesbeck, O., G. S. Baird, R. E. Campbell, D. A. Zacharias, and R. Y. Tsien. 2001. Reducing the environmental sensitivity of yellow fluorescent protein. Mechanism and applications. *J. Biol. Chem.* 276: 29188–29194.

10. Kuner, T., and G. J. Augustine. 2000. A genetically encoded ratiometric indicator for chloride: capturing chloride transients in cultured hippocampal neurons. *Neuron.* 27:447–459.

11. Ormo, M., A. B. Cubitt, K. Kallio, L. A. Gross, R. Y. Tsien, and S. J. Remington. 1996. Crystal structure of the *Aequorea victoria* green fluorescent protein. *Science.* 273:1392–1395.

12. Goslin, K., H. Asmussen, and G. Banker. 1998. Rat hippocampal neurons in low-density culture. *In* Culturing Nerve Cells. MIT Press, Cambridge, MA. 339–370.

13. Berman, H. M., J. Westbrook, Z. Feng, G. Gilliland, T. N. Bhat, H. Weissig, I. N. Shindyalov, and P. E. Bourne. 2000. The Protein Data Bank. *Nucleic Acids Res.* 28:235–242.

14. Sauder, M. J. 1999. Blast 2 model, 1.0. Fox Chase Cancer Center, Philadelphia, PA.

15. Brunger, A. T. 1988. X-PLOR, 3.1. HHMI, DMBB, Yale University, New Haven, CT.

16. Guex, N., and M. C. Peitsch. 1997. SWISS-MODEL and the Swiss-PDBViewer: an environment for comparative protein modeling. *Electrophoresis.* 18:2714–2723.

17. Vriend, G. 1990. WHAT IF: a molecular modeling and drug design program. *J. Mol. Graph.* 8:52–56.

18. Laskowski, R. A., J. A. Rullmann, M. W. MacArthur, R. Kaptein, and J. M. Thornton. 1996. AQUA and PROCHECK-NMR: programs for checking the quality of protein structures solved by NMR. *J. Biomol. NMR.* 8:477–486.

19. Lippincott-Schwartz, J., and G. H. Patterson. 2003. Development and use of fluorescent protein markers in living cells. *Science.* 300:87–90.

20. Kemnitz, K., L. Pfeifer, R. Paul, and M. Coppey-Moisan. 1997. Novel detectors for fluorescence lifetime imaging on the picosecond time scale. *J. Fluor.* 7:93–98.

21. Beechem, J. M., and E. Haas. 1989. Simultaneous determination of intramolecular distance distributions and conformational dynamics by global analysis of energy transfer measurements. *Biophys. J.* 55:1225–1236.

22. Lakowicz, J. R. 1999. Principles of Fluorescence Spectroscopy. Kluwer Academic/Plenum Publishers, New York.

23. Patterson, G. H., D. W. Piston, and B. G. Barisas. 2000. Forster distances between green fluorescent protein pairs. *Anal. Biochem.* 284:438–440.

24. Kapusta, P., R. Erdmann, U. Ortmann, and M. Wahl. 2003. Time-resolved fluorescence anisotropy measurements made simple. *J. Fluor.* 13:179–183.

25. Gulyas, A. I., A. Sik, J. A. Payne, K. Kaila, and T. F. Freund. 2001. The KCl cotransporter, KCC2, is highly expressed in the vicinity of excitatory synapses in the rat hippocampus. *Eur. J. Neurosci.* 13: 2205–2217.

26. Miyawaki, A., J. Llopis, R. Heim, J. M. McCaffery, J. A. Adams, M. Ikura, and R. Y. Tsien. 1997. Fluorescent indicators for Ca^{2+} based on green fluorescent proteins and calmodulin. *Nature.* 388:882–887.

27. Habuchi, S., M. Cotlet, J. Hofkens, G. Dirix, J. Michiels, J. Vanderleyden, V. Subramaniam, and F. C. D. Schryver. 2002. Resonance energy transfer in a calcium concentration-dependent Cameleon protein. *Biophys. J.* 83:3499–3506.

28. Bevensee, M. O., T. R. Cummins, G. G. Haddad, W. F. Boron, and G. Boyarsky. 1996. pH regulation in single CA1 neurons acutely isolated from the hippocampi of immature and mature rats. *J. Physiol.* 494:315–328.

29. Llopis, J., J. M. McCaffery, A. Miyawaki, M. G. Farquhar, and R. Y. Tsien. 1998. Measurement of cytosolic, mitochondrial, and Golgi pH in single living cells with green fluorescent proteins. *Proc. Natl. Acad. Sci. USA.* 95:6803–6808.

30. Tramier, M., K. Kemnitz, C. Durieux, and M. Coppey-Moisan. 2004. Picosecond time-resolved microspectrofluorometry in live cells exemplified by complex fluorescence dynamics of popular probes ethidium and cyan fluorescent protein. *J. Microsc.* 213:110–118.

31. Nair, D. K., M. Jose, T. Kuner, W. Zuschratter, and R. Hartig. FRET-FILM at nanometer spectral resolution from living cells. *Optics Express.* 15:12217–12229.

32. Borst, J. W., M. A. Hink, A. van Hoek, and A. J. Visser. 2005. Effects of refractive index and viscosity on fluorescence and anisotropy decays of enhanced cyan and yellow fluorescent proteins. *J. Fluor.* 15:153–160.

33. Guerrero, G., and E. Y. Isacoff. 2001. Genetically encoded optical sensors of neuronal activity and cellular function. *Curr. Opin. Neurobiol.* 11:601–607.

34. Birks, J. B. 1970. Photophysics of Aromatic Molecules. John Wiley & Sons, New York.

35. Rizzo, M. A., G. H. Springer, B. Granada, and D. W. Piston. 2004. An improved cyan fluorescent protein variant useful for FRET. *Nat. Biotechnol.* 22:445–449.

36. Zapata-Hommer, O., and O. Griesbeck. 2003. Efficiently folding and circularly permuted variants of the Sapphire mutant of GFP. *BMC Biotechnol.* 3:5.